Addis Ababa University
አዲስ አበባ ዩኒቨርሲቲ
Seek Wisdom, Elevate your Intellect and Serve Humanity

College Of Natural and Computational Sciences

School of Earth Sciences

Remote Sensing and Geoinformatics

Stream

Thesis submitted to School of Earth sciences for the partial fulfillment of masters of Science in Remote sensing and Geo informatics

Detection and mapping landslides using Persistent Scatterer Interferometry method and Sentinel 1 SAR data, Dessie area, Ethiopia

By: **Abel Mesele**
(ID: GSR/9524/15)

Advisor: **Dr. Binyam Tesfaw**

Addis Ababa University
May 2024

Table of Contents

No. **List of Figures** Page

List of Tables

List of Acronyms

AHP	Analytical Hierarchical Process
CHIRPS	Climate Hazards Group Infrared Precipitation
DEM	Digital Elevation Model
FAO	Food and Agricultural Organization
GIS	Geographic Information Systems
GEE	Google Earth Engine
GPS	Global Positioning System
Ha	Hectare
INSAR	Interferometric Synthetic Aperture Radar
LHZ	Landslide Hazard Zonation
LULC	Land Use Land Cover
PS	Persistent Scatterer
PSI	Persistent Scatterer Interferometry
ESA	European Space Agency
SAR	Synthetic Aperture Radar
SLC	Single-look complex
SSGI	Space Science and Geospatial Institute
USGS	United States of Geological Survey
UTM	Universal Transverse Mercator

Acknowledgements

I express my profound gratitude to the Almighty for bestowing upon me health, peace, knowledge, and wisdom, enabling me to complete this thesis work.

I wish to express my deep gratitude to Dr. Binyam Tesfaw, my esteemed advisor, for his invaluable guidance and unwavering encouragement during the course of this thesis work. His patience, expertise, and friendship have played pivotal role in the successful completion of this endeavor. His adeptness in scientific writing focusing specifically on technical aspects has been particularly illuminating and enriching.

Special thanks are due to my instructors, Professor K.V. Suryabhagavan and Dr. Tibebu Kassawmar, as well as all the faculty members of Addis Ababa University, School of Earth Sciences, for their support in imparting knowledge of Hydrology, Geology, Remote Sensing, and GIS.

I also acknowledge the Ethiopian National Meteorological Agency, Ethiopian Geological Survey, and Space science and geospatial institute for providing crucial data and resources essential for my research.

Lastly, I extend my heartfelt appreciation to my friends Workineh Tesfaye, Jerbaw Tiruneh, Andinet Nigussie and Haile Alemu, for their unwavering support and guidance. Additionally, I am thankful to all my colleagues in the Remote Sensing and Geoinformatics stream for their friendship and collaboration.

Detection and mapping landslides using Persistent Scatterer Interferometry method and Sentinel 1 SAR data, Dessie area, Ethiopia
Abel Mesele, MSc Thesis
Addis Ababa University, May 2024

Abstract

One of the highly destructive natural disasters is landslide and pose a serious threat to the safety of people, property, and the social and economic development. In a country like Ethiopia, with a high rugged topography and population, landslide hazard became a threat especially in the highland areas, most populated and surrounding regions. Hence, effective landslide monitoring with high precision and real-time capabilities required to implement proactive measures for disaster preparedness and mitigation. Therefore, a comprehensive approach using Interferometric Synthetic Aperture radar (InSAR) interferometry data is crucial to address the existing gaps in utilizing field survey and optical remote sensing and enhance the understanding of landslide dynamics. This study aims to study and map the surface displacement and to improve the landslide hazard zonation mapping in Dessie town and surrounding Ethiopia. The research used the Persistent Scatterer (PS) InSAR method and Sentinel 1 SAR data in SARPROZ and ArcGIS software. The results were validated using the Landslide inventory from 15 points collected from field observation and secondary data. Eight parameters or factors were identified such as slope, aspect, elevation, lithology, rainfall, land-use, and land-cover, distances from river and road as causes for the occurrence of landslide in the area. The deformation results indicated a maximum displacement (subsidence) of 64.1 mm and a minimum of 19.8 mm/year, with maximum velocity of 0.38 mm per year. The landslide zonation map result shows 1797.09 ha (20.57%), 1716.19ha (19.64%), and 1721.53 ha (19.71%) covered by medium, high, and very high susceptibility, respectively. In addition, most of the high and very high hazard zones are located on north east, central and south west parts of the study area, these areas are directly connected to the topography. Validation results show that (80%) of inventory points are located in high and very hazardous zones. This comprehensive (hybrid) and technologically advanced approach provides valuable insights into landslide occurrences in the study area, aiding in effective hazard assessment and mitigation strategies for the region.

Keywords: Displacement, PSInSAR, Landslide, Landslide hazard zone, SARPROZ, Sentinel 1.

CHAPTER ONE

1. Introduction

1.1 Background of the Study

Landslides are highly destructive natural disasters that pose a serious threat to the safety of people, property, and the social and economic development making them an immensely destructive natural calamity (Mengistu et al., 2019; Sim et al., 2022). Mass movement strategies have the potential to induce remarkable transformations within the Earth's topography, resulting in significant economic repercussions caused by landslides in densely populated mountainous regions (Dubey et al., 2023). Moreover, these strategies can also lead to significant direct and indirect costs associated with the destruction of buildings and infrastructure on an urban level (Sim et al., 2022). Landslides are considered internal processes in relief development and, among other things, promote the formation of valleys (Carrión-Mero et al., 2021), and the contribution of river sediments to ecological renewal is significant. Various natural processes such as physical, biological, and chemical weathering, earthquakes, and abnormal rainfall can result in slope instability (Nanehkaran et al., 2023). Around the world, landslides have resulted in expensive damage and fatalities, but the most catastrophic events happen in developing nations (Sim et al., 2022)

Landslides pose a significant risk to both human life and property on a global scale, and the mountainous areas are particularly vulnerable to these catastrophic events (Nanehkaran, 2023). For the past twenty years, China has experienced a consistent annual death toll of approximately 1000 individuals due to landslides, along with substantial economic losses (Huang, 2009). The identification of the slope as a hazardous geohazard was not done prior to the catastrophic event. This lack of identification can be attributed to the difficulties faced in conducting geological field investigations at its high-altitude location (Peng, 2023). Hence, it is of utmost importance to give priority to the detection and regular monitoring of slope instabilities in areas with complex topography such as mountains and valleys. This will help ensure the safety of human lives and infrastructure by mitigating the risks associated with potential landslide disasters.

In the recent past, Ethiopia has been progressively impacted by landslide hazard especially in the highland areas and surrounding regions (Bekele Abebe et al., 2010). These locations are particularly prone to landslides due to the rapid population increase (Ahmed, 2020; Awoke, 2021; Tilahun and Matebie, 2020). Ethiopia has to put sustainable land management practices first, make preparations for disasters, and put in place efficient response systems in order to lessen the effects of landslides and protect the general public. Its population and infrastructure will be protected, and hazards will be reduced (Abay et al., 2019). Consequently, in order to identify and manage areas at risk and aid in the planning of future urban projects, the ability to detect ground deformation associated with landslides will continue to be essential.

Monitoring of landslides usually one way to identify unstable slopes is to measure the surface deformation, which is a characteristic that sets landslides apart. Landslide movements have conventionally been assessed through various techniques such as inclinometers, extensometers, total stations, GPS, and the examination of geomorphological data (Jie et al., 2018; Ruzza et al., 2020). These onsite observation devices, although accurate, are usually designed for closely monitoring particular, well-defined landslides. Nevertheless, their usage is restricted in terms of coverage, making them less efficient in detecting and analyzing landslides over large areas. Through the interpretation of surface characteristics, optical remote sensing allows for rapid and comprehensive mapping of landslides (Casagli et al., 2023; Lissak et al., 2020), However, these tools often struggle to detect the very subtle movements associated with slow-moving landslides.

Satellite InSAR possesses an inimitable ability to measure small ground deformation with great precision (Hrysiewicz et al., 2023; Jie et al., 2018; Necula et al., 2021). Over the past decade, Interferometric Synthetic Aperture Radar (InSAR), particularly through time series InSAR analysis, has gained prominence for mapping and monitoring landslide movements on a larger scale (Natnael and Solomon 2023; Bayer et al., 2017; Liu et al., 2022; XIE et al., 2019; www.usgs.gov). References contain comprehensive reviews of the various applications of InSAR in landslide investigations (Francesco et al., 2023: Solari et al., 2023). A significant number of such applications were concentrated in Europe and the United States. Moreover, extensive research was carried out on the regional InSAR landslide detection in China, specifically focusing on the Three Gorges Reservoir area (Lichuan et al., 2020: Shi et al., 2016) and the Bailong River Basin (Li et al., 2021; Liu et al., 2023; Zhang et al., 2016).

1.2 Statement of the problem

A landslide is an inherent movement of a slope that occurs due to topographical, geological, and hydrogeological phenomena. In addition to the causing factors landslide can be also triggered by various initiating factors such as rainfall, seismicity, and volcanism (Raghuvanshi et al., 2014). It significantly contributes to the ongoing process of mountain transformation (Cong et al., 2021). The present study area, known for its rugged terrain and susceptibility to landslides, demands effective monitoring and management strategies. However, conventional methods of landslide detection and mapping often prove inadequate in providing timely and accurate information for mitigation and preparedness. The utilization of InSAR (Interferometric Synthetic Aperture Radar) technology, in conjunction with data from the Sentinel 1 satellite, holds great potential as an effective approach for monitoring landslides in real-time and creating accurate maps. This innovative solution offers significant benefits in terms of providing valuable information for disaster management and reducing risks in the Dessie region.

Despite the potential of advanced remote sensing technologies, the Dessie area continues to encounter the challenge of timely and accurate landslide detection and mapping. Traditional methods based on field surveys and optical remote sensing lack the precision and real-time capabilities required for effective landslide monitoring. This limitation hampers the region's ability to implement proactive measures for disaster preparedness and mitigation. Thus, a comprehensive approach utilizing InSAR interferometry with Sentinel 1 data is critical to address the existing gaps and enhance the understanding of landslide dynamics in the Dessie area.

1.3 Objectives

1.3.1. General objective

The main objective of the study was to detect and map landslide occurrences in the Dessie area using satellite image from Sentinel–1 SAR interferometry.

1.3.2. Specific objectives

- To prepare inventory mapping of past and current landslide events using primary field and secondary data.
- To map the landslide triggering factors and evaluating their importance for the occurrence of landslides.
- To quantify and validate the deformation using Sentinel 1 SAR interferometry, correlation analysis with the existing landslides and mapping the landslide zonation.

1.4 Research Questions

Based on the above stated specific research objectives, the following leading research questions are drawn.

- ✓ What are the temporal and spatial distribution of past and current landslide events in Dessie, Ethiopia?
- ✓ What are the specific aspects that contribute to landslides in the Dessie area?
- ✓ How can the accuracy and reliability of InSAR interferometric techniques be validated and improved through the integration of field and secondary data in the Dessie, Ethiopia?

1.5 Scope of the study

The geographical and thematic boundaries of this study were restricted. Specifically, the study was concentrated on the city of Dessie, with a particular emphasis on identifying and mapping landslide movements. The primary approach employed in this study involved the utilization of InSAR interferometry, utilizing data from Sentinel-1A, to effectively detect and map landslides within Dessie City, and a landslide hazard zonation map was prepared to identify susceptibility classes

1.6 Significance of the study

The utilization of advanced InSAR technology and Sentinel 1 data in this study will play a crucial role in enhancing the understanding of landslide dynamics in the Dessie area. The research findings will offer valuable insights to local authorities, urban planners, and disaster management agencies, enabling them to develop effective strategies for assessing landslide risks, implementing early warning systems, and enhancing disaster preparedness. Moreover, the outcomes of this study will contribute to the existing knowledge on remote sensing applications for managing natural hazards. This will pave the way for the integration of advanced technologies in disaster risk reduction initiatives in other regions prone to landslides worldwide.

1.7 Limitations of the thesis

The present study made every attempt to obtain the information required for the primary and secondary data collection, analysis, and interpretation processes, but the study had some limitations: The unwillingness of organizations to provide secondary data quickly; the absence of either an ascending or descending SAR dataset; downloading Sentinel 1A (S-1A) data from the

Copernicus website; Processing SAR data requires a significant amount of storage and a powerful computer, and it is more sensitive to vertical displacement than horizontal displacement. Nevertheless, this study provides important information and useful data that are essential for assessing the hazards of landslides.

1.8 Organization of the thesis

The thesis consisted of five distinct chapters, chapter one encompassing an introduction, chapter two literature review, chapter three methodology, chapter, chapter four results and discussion, chapter five conclusion and recommendations. Each chapter served a specific purpose within the research process and contributed to the overall aim of the study. The first chapter, the introduction, provided an overview of the research topic, introduced the study's objectives, and highlighted the significance of the research. Moving on to the second chapter, the literature review, an extensive examination of existing literature pertaining to the research topic was conducted. The third chapter, methodology, outlined the research methodology employed to gather data, including the research design, data collection methods, and data analysis techniques. In the fourth chapter, results, analysis and discussion, the research findings were presented and thoroughly analyzed. This chapter involved the interpretation of collected data, statistical analyses, and the use of graphs and tables to support the findings. Finally, the fifth chapter, conclusion and recommendations, offered a comprehensive discussion of the research findings in relation to the research objectives. It critically analyzed the results, compared them with existing literature, and drew conclusions based on the findings.

CHAPTER TWO

2. Literature Review

2.1. Landslide: an overview

A landslide represents the downward movement of materials such as rocks and soil along a curved (known as a rotational slide) or flat (referred to as a translational slide) surface. During this geological event, the materials involved often travel in a consolidated or semi-consolidated block, exhibiting minimal internal distortion. It is important to recognize that landslides can sometimes encompass a range of movement types. This variability can occur initially at the moment of failure or subsequently as the properties of the displaced material evolve while it travels downslope (Highland and Bobrowsky, 2018). Landslides are indicators of slope instability, which refers to the propensity of a slope to experience deformation or disruption through landslide phenomena. This instability can manifest in several forms of natural hazards, including rockfalls, rockslides, debris flows, soil slips, rock avalanches, and mudflows, each varying in their characteristics and potential impact (Fayera, 2020). A landslide is a term used to describe various processes that result in the visible movement of soil, rock, and vegetation down and away from a slope due to the force of gravity (Wubalem, 2022). Landslides play a significant role in shaping the mountainous landscapes through mass wasting and landform development (Andsera et al., 2022). The materials might also additionally pass through falling, toppling, sliding, spreading, or flowing (UNISDR, 2017).

Landslides and slope deformations in the Ethiopian Rift margins and surrounding highlands are valuable resources for researchers (Abebe et al., 2010; Mebrahtu et al.,2021; Abay et al., 2019). Landslides, like other natural events, can be caused by natural forces or human activities related to development. These triggers have the potential to alter the natural landscape and environment (Michele,2023).

2.2. Types of landslides

Landslides can be categorized into different types based on the type of movement and the type of material involved (Highland and Bobrowsky, 2018). According to certain individuals, the classification of landslides is based on the distinct internal mechanisms responsible for the movement of a mass of soil or rock. These movement types encompass fall, topple, slide, spread, or flow. Consequently, landslides are identified by terms that describe both their composition and manner of movement, such as rock fall or particle flow (Highland and

Bobrowsky, 2018). Fayera (2020) stated in his thesis that movements with a velocity > 5m/s are considered extremely rapid, while those < 16mm/yrs. are considered extremely slow.

Varnes (1978) proposed the most widely used classification for landslides, which was also adopted by the Landslide Committee of the Highway Research Board in Washington. This classification categorizes landslides into falls, topples, slides, lateral spreads, and flows, and also distinguishes between different types of materials such as soil, debris, and bedrock. These materials have the potential to move through various mechanisms including falling, toppling, slumping, sliding, spreading, or flowing. In 1978, Varnes classified the major types of slope failures as creep, slide, fall/topple, flow, and spread present in Table 1.

Table 1: Slope movement classification (Varnes, 1978)

Movement type			Types of materials		
			Bedrock	Engineering soils	
				Predominantly Coarse (debris)	Predominantly fine (earth)
Falls			Rock fall	Debris fall	Earth fall
Topples			Rock topples	Debris topples	Earth topples
Slides	Rotational	Few unit	Rock slump	Debris slump	Earth slump
	Translation	Manyunits	Rockslides	Debris slides	Earth slides
Lateral spread			Rock spread	Debris spread	Earth spread
Flows			Rock flow (Deep creep)	Debris flow (soil creep)	Earth flow
Complex (Combination of two or more types of movement)					

I. Falls

Falls are sudden occurrences in which significant amounts of geological materials, including rocks and boulders, separate from steep slopes or cliffs. This separation takes place along fractures, joints, and bedding planes, and the movement is characterized by a free downward descent, rebounding, and rolling. The forces of gravity, mechanical weathering, and the presence of water within the materials all play significant roles in influencing falls (Varnes, 1978).

II. Topple

Toppling failures occur when a unit or multiple units rotate forward around a pivotal point, typically located below or low within the unit. These rotations are caused by the combined forces of gravity and pressure from adjacent units or fluids within cracks (USGS, 2023).

III. Slide

A landslide occurs when a large amount of soil or rock moves downwards along surfaces that have experienced rupture or narrow zones with considerable shear strain. In a rotational landslide, the surface of rupture takes on a curved, spoon-shaped form, and the slide primarily rotates around an axis that is parallel to the contour of the slope. On the other hand, in a translational landslide, the mass moves outward or downward along a relatively flat surface, with minimal rotational motion or backward tilting. Translational slides often happen along geological features such as faults, joints, bedding surfaces, or the boundary between rock and soil (USGS, 2004).

IV. Flow

According to the United States Geological Survey (USGS, 2004), there exist five main categories of flows that display unique characteristics from each other.

Debris flows: A debris flow refers to a swift and powerful movement of a mixture consisting of loose soil, rocks, organic matter, air, and water. This mixture transforms into a slurry that flows downhill. Typically, these flows contain less than 50% fine particles. Debris flows are commonly triggered by intense surface-water flow resulting from heavy rainfall. Additionally, they can be triggered by rapid snowmelt, which leads to erosion and the mobilization of loose soil or rock on steep slopes. They can also originate from other types of landslides occurring on saturated slopes, where a significant portion of the material is composed of silt and sand. The initiation areas of debris flows are often associated with steep gullies, and the presence of debris fans at the mouths of these gullies indicates the deposition of debris flows. Moreover, slopes that have been stripped of vegetation due to fires are more susceptible to debris flows.

Debris avalanche: This kind of debris flow exhibits a range from very quick to extremely quick movement.

Earth flow: Earth flows are known for their unique "hourglass" form. The substance on the incline transforms into a liquid state and moves outward, resulting in a depression or concave feature at the origin. The flow itself is elongated and commonly transpires in fine-grained materials or clay-rich rocks on moderate slopes when the circumstances are saturated. Nevertheless, it is also feasible for dry flows to transpire with granular substances.

Mudflow: A mudflow is a specific form of earth flow distinguished by the swift movement of material that is adequately moist and comprises at least 50 percent particles of sand, silt, and clay sizes. It is important to mention that in certain instances, like in newspaper articles, mudflows and debris flows are frequently labeled as "mudslides."

Creep: Creep is the term used to describe the gradual and slow downward displacement of soil or rock on slopes. This displacement happens at an extremely slow rate and is caused by shear stress that is strong enough to cause permanent deformation, yet not strong enough to lead to shear failure. Typically, there are three distinct types of creep:

- ✓ Seasonal creep occurs in the soil layer that is influenced by variations in soil moisture and temperature throughout the seasons.
- ✓ Continuous creep takes place when the shear stress consistently surpasses the material's strength.
- ✓ Progressive creep is observed when slopes are nearing the point of failure, resembling other forms of mass movements.

Indications of creep consist of tree trunks with a curved shape, fences or retaining walls that are bent, poles or fences that are tilted, and slight ripples or ridges in the soil (USGS, 2023).

V. Lateral spreads

Lateral spreads tend to be common on mild slopes or flat terrain, making them most noticeable in these types of environments. The primary mechanism of movement is longitudinal extension, which is accompanied by shear or tensile fractures. These failures are often caused by liquefaction, a process in which saturated, loose sediments with little cohesiveness (such as sands and sediments) change from solid to liquid form. Sudden ground motion, like that felt following an earthquake, is a common trigger, but artificial factors can also cause failure. When a cohesive material, such as bedrock or soil, is supported by liquefiable materials, its uppermost layers may fracture, extend, subside, translate, rotate, disintegrate, or even liquefy and flow. Progressive lateral spreading is common in materials with fine grains on steep slopes. The collapse begins abruptly in a limited area and quickly spreads. While the first sign of failure may emerge as a slump, movement can occur without any obvious cause. A complicated landslide is a combination of two or more of the aforementioned types (USGS,2004).

According to Cruden and Varnes (1996), the complicated type of movement might result in a combination of several different kinds of failure on a single slope. This form of failure can occur simultaneously or throughout a slope's lifetime.

2.3. Factors that trigger landslides

There are two basic causes of landslides: inner forces and outside triggering events. Inner factors include slope geometry, material composition, architectural discontinuities, land use and cover, and groundwater. Outside triggering variables include seismic activity, rain, and activities by humans (Gizawu, 2020). Landslide hazard evaluation takes into account lithology, closeness to the fault, land use, slope steepness, aspect, elevation, and proximity to drainage (Abay e al., 2019).

Internal parameters are the causative characteristics that determine whether the slope is stable or unstable. These inherent variables include the geometry of the slope, material of the slope, structural discontinuities, land use/cover, and groundwater (Oyda and Regasa, 2023). The primary causes of landslides include slope material, slope, aspect, elevation, land use, land cover, and groundwater-surface traces (Kumar et al., 2015).

2.3.1. Elevation

As various studies have shown, elevation is an important element in determining landslide risk (Abay et al., 2019). Landslides are mostly triggered by elevation, which determines the level of weathering, humidity change, the velocity of hydrate reaction, erosion processes, and weathering depth. It is considered that outside events become more intense as altitude increases. These external activities might destabilize the slope surface, increasing the danger of landslides (Kova et al., 2017).

2.3.2. Slope

The slope steepness is a major element in causing landslides. In several landslide investigations, slope steepness is identified as the principal cause of landslides. Slope morphometry maps categorize slopes according to the prevalence of distinct slope angles. The order of appearance of these slope types is governed by an area's geomorphological history. Each slope angle indicates a set of localized processes and controls that have shaped the landform (Asmelash, 2012).

2.3.3. Aspect

Aspect is the orientation of the steepest slope along the surface of the ground about the north (George and Vayia, 2018). The aspect of a slope has a considerable impact on triggering landslides because it influences parameters such as moisture retention, vegetation cover, soil strength, and landslip susceptibility (Mekonnen et al., 2022).

2.3.4. Curvature

The word "curvature" is described in theory as a measure of how the gradient of the slope or aspect changes, usually in one direction (Vincenzo et al., 2019). Curvature values provide insights into the morphology of the topography. Negative curvature indicates upward concavity at a given raster cell, while positive curvature suggests upward convexity. A curvature value of zero represents a flat surface. The likelihood of landslide activity tends to increase with more negative curvature values. Typically, hilly and mountainous areas exhibit higher curvature values, while flat areas have lower values (Psomiadis et al., 2020).

2.3.5. Proximity to lineament

According to the studies done by (Hussin et al., 2017; Chen et al., 2017) Lineaments are identifiable linear features found on the Earth's surface, indicating zones of weakness and structural discontinuities in rocks. These lineaments affect the makeup of surface materials, as well as topography and permeation, which affect slope stability. The proximity of a slope to these characteristics influences its stability, with closer proximity increasing the risk of landslides. Geological faults and areas with jointed rock are particularly prone to landslides since the strength of the surrounding rock decreases due to tectonic fractures. As a result, lineaments can contribute to landslide development, with the risk decreasing as the distance from lineament structures rises.

2.3.6. Proximity to drainage

The closeness of slopes to drainage infrastructure is an important aspect of determining the stability of a slope. Rivers may be unstable by eroding the slopes or saturating the bottom section of the material, resulting in increased water levels (Çellek, 2019). The distance from a stream is a significant variable that determines the stability of a slope. Proximity to rivers can lead to the failure of slope banks owing to undercutting, and the modification of soil structure caused by gully erosion can also influence the initiation of landslides (Wendim et al., 2023).

2.3.7. Lithology

Lithology is a necessary observation in the survey of landslides because different lithological strata have dissimilar degrees of susceptibility. Therefore, it is essential to consider lithology. The occurrence of landslides is significantly influenced by lithology, as differences in lithological content can result in variances in the resistance and porosity of rocks and soils (Abay et al., 2019; Henriques, et al.,2015).

2.3.8. Soil properties

Soil properties have a significant impact on the frequency of landslides. Landslides may happen when the soil's moisture content exceeds the maximum amount of liquid in the landscape. That can have serious and perhaps fatal implications since seemingly stable soil can suddenly give way under stress. When the moisture content of the soil increases, it weakens the soil by reducing capillary cohesion (Nseka, et al., 2022)

2.3.9. Proximity to roads

According to (Ayalew and Yamagishi, 2005) road-cuts often contribute to unstable conditions caused by human activities. These road segments can function as barriers, sources or sinks of water flow, or even serve as pathways for water movement. In mountainous regions, roadways can cause landslides. While some slope failures occur above highways, they are often caught by roadway structures.

2.3.10. Land-use and land-cover

Landcover encompasses the different physical materials found on the Earth's surface, including grass, asphalt, trees, bare ground, and water. Conversely, land use pertains to the intentional management and modification of the natural environment or undeveloped areas into human-made environments like settlements, as well as semi-natural habitats such as cultivated fields, pastures, and well-maintained forests (Offiong, et al., 2018).

Land cover is an important factor in determining slope stability. Areas with sparse vegetation or barren land are more susceptible to erosion and therefore, more prone to instability and mass wasting processes. In contrast, reserve or protected forests with thick vegetation are less likely to experience landslides. Land use and the type of land covering it have a considerable impact on the possibility of landslides. Landslides are more likely to occur in regions with dense vegetation than in places with less vegetation, agricultural, or urban development (Pacheco et al., 2023).

2.3.11. Rainfall

Landslides can happen for a variety of reasons, including the frequency and intensity of rainfall events, as well as the geological composition of the land, the shape of the terrain, and the type of vegetation covering it. Heavy rainfall, in particular, is identified as the primary factor that triggers landslides in almost all cases (Broothaerts et al., 2012). The instability of slopes is directly influenced by the intensity of rainfall. As a result, most landslides happen during the rainy season. Rainfall not only causes surface erosion but also replenishes groundwater, leading to the saturation of slope materials. This increased saturation contributes to the susceptibility of slopes to landslides (Addisalem, 2017).

2.4. Methods of Landslide hazard zonation mapping

Landslide hazard zonation is important in understanding landslides, managing them, and developing sustainable land use plans. It entails determining the numerous elements that produce and trigger landslides. By conducting landslide hazard zonation, we can investigate landslides, effectively manage the associated risks, reduce catastrophic losses, and formulate guidelines for sustainable land use management (Mengistu et al., 2019). Landslide hazard zonation (LHZ) is important for identifying areas at risk of landslides and other mass movements. It helps to understand the connection between landslides and their causes, as well as ranking areas based on their susceptibility to both current and future hazards. This process aids in predicting and assessing landslide hazards in the future (Hamza and Raghuvanshi, 2017). The various landslide hazards zonation approaches are explained as follows:

2.4.1 Analytic Hierarchy Process (AHP)

The Analytic Hierarchy Process developed by Saaty, (1977), is a helpful instrument for making a decision. It enables decision-makers to prioritize and make educated choices about challenging issues. AHP divides these complicated choices into a hierarchy of criteria and alternatives, simplifying the method of making choices with pairwise comparisons. By combining rational and intuitive elements, AHP helps determine the most effective alternative based on multiple criteria. It also ensures consistency in the decision maker's evaluations while allowing for some degree of inconsistency.

The AHP employs a set evaluation criteria and alternatives to make effective decisions. It calculates weights for each criterion through pairwise comparisons. Higher weights mean more importance. It assigns scores to options based on comparisons against criteria. Higher scores mean better performance. The information is organized in a hierarchical tree structure. The AHP generates global scores for options by combining criteria weights and option scores. This process determines relative rankings. Implementing AHP involves three simple steps.

The steps are:

a. Calculate the weight vector for all criteria.
b. Calculate the score matrix for all options.
c. Rank the options based on the final score.

The AHP is a general theory of measurement. It helps determine the priorities of different criteria. This is done on absolute scales. Pairwise comparisons of criteria and/or options are conducted using the scale in Table 2.

Table 2. Fundamental scale of the AHP by Saaty (1977)

Scale	Definition	Explanation
1	Equal significance	Two activities have an equal impact on the objective.
2	Week	
3	Moderate significance	Experience and judgment incline somewhat towards one activity over the other.
4	Moderate plus	
5	Strong significance	Experience and judgment strongly support one activity as preferable to another.
6	Strong plus	
7	Very strong	An activity is greatly favored over another; this is proved in practice.
8	Very, very strong	
9	Extreme significance	The evidence supporting one action over another is at the highest level of certainty.

Several researchers have utilized this method of decision-making to allocate weights to different factors affecting the occurrence of landslides. The impact of each factor and factor category on landslide occurrence is assessed through pairwise comparison, and an equation is formulated to calculate the landslide susceptible index (LSI), as shown in the following equation.

$$\boldsymbol{LSI_{AHP}} = \sum_{i=1}^{n} . \boldsymbol{Factor\_i} * \boldsymbol{W_{AHP\_i}} \tag{1}$$

where Factor *i* is Landslide conditioning factors include lithology, slope, and aspect, etc. W_{AHPi} is Weight of each causative element. The pixel (LSI) values obtained from the preceding equations are divided into susceptibility classes (low, moderate, high, and extremely high) based on natural break.

2.4.2. Landslide inventory mapping

Landslide inventory mapping, also known as distribution analysis, is a straightforward technique for qualitative mapping of landslide susceptibility. This strategy involves gathering data about landslides from several sources, such as historical records, field surveys, aerial photo interpreting, and satellite imagery (Shano et al., 2020). The information including location, dimension, type, and magnitude of the landslides are documented in inventory analysis. The resulting landslide inventory map depicts slope failures caused by a single incident or the combined impacts of numerous occurrences (Azemeraw, 2021). To accurately estimate the hazard of landslides, it is crucial to have a comprehensive understanding of the historical occurrences in the area. This includes identifying the types of landslides that have taken place and the factors that triggered them. In the Gechi district, several landslide incidents have occurred in the past, resulting in the development of a database of landslides. As part of this research, information from the landslide database was gathered and utilized to produce a comprehensive inventory map (Kumar et al., 2015).

2.4.3. Statistical approach

Landslide hazard assessment often involves the use of statistical methods to analyze geo-environmental factors associated with landslides. These methods aim to reduce bias by focusing on causal factors. Two main statistical approaches for mapping landslide hazards are bivariate statistical analysis and multivariate statistical analysis. These approaches evaluate the spatial susceptibility of landslides by examining the connection between landslide occurrences and contributing factors (Tilahun and Raghuvanshi, 2017).

2.4.3.1. Bivariate statistical approach

Weight values for landslide hazards can be calculated using a variety of statistical methods, including the information value method, fuzzy logic, Bayesian combination rules, the Dempster-

Shafer method, weights of evidence modeling and certainty factors. This approach assesses the magnitude or impact of each contributing element toward landslide hazard by considering landslide density. Geographic Information Systems play a significant role in this process, which includes categorizing parameter maps into appropriate classifications, determining landslide density, processing thematic maps, and giving weights to different parameter maps. The bivariate technique compares causal factors to existing landslides and allocates weights based on their severity and distribution. However, one limitation of this approach is the interdependence of many parameter maps about landslide likelihood (Gebremicheal, 2017).

2.4.3.2. Multivariate statistical analysis

Multivariate statistical analysis is used to map landslide hazard zoning and examine how each thematic data layer affects overall landslide susceptibility. Includes determining the percentage of landslide-prone areas in each pixel and distinguishing non-prone landslides. By generating a presence data layer, a multivariate statistical method is then applied to reclassify the hazard for the specific area. Several methods are routinely used for this purpose, including logistic regression, determinant analysis, multiple regression models, conditional analysis, and artificial neural networks (ANN). These methods aid in correctly mapping and assessing the hazard potential of landslides in a given location (Pardeshi, et al., 2013).

2.4.4. Artificial Neural Network (ANN)

Artificial Neural Networks are frequently used in the creation of Landslide Hazard Zone (LHZ) maps. Researchers have used several variations of ANN designs, which typically consist of a single input layer, a pair of hidden layers, and one output layer, to investigate the numerous elements that influence landslide occurrences. The ANN's connection weights are then utilized to assign weights or rankings to the input data sources, which indicate the factors that contribute to landslides. By integrating these weights and rankings of categories, a comprehensive Landslide Susceptibility Zonation (LSZ) map can be generated. This approach allows for the effective incorporation of multiple factors and provides valuable insights for landslide hazard assessment and management (Salamat et al., 2022).

2.4.5. Deterministic approach

The deterministic approach is used to assess landslide hazards by providing precise values in terms of safety factors or probabilities. Quantitative analyses are typically used for small to medium-sized areas on a large to medium scale. However, they require a significant amount of detailed input data, and the lack of complete data may result in oversimplification (Beyene, 2016). Furthermore, applying deterministic numerical methods to large areas may not be cost-effective.

2.5. Surface deformation monitoring with SAR

Synthetic Aperture Radar is a remote sensing technology that uses radar to create high-resolution images of the Earth's surface. SAR creates comprehensive radar images by emitting microwave frequencies then analyzing the signals that return. This technology operates day and night, unaffected by cloud cover, making it ideal for areas with frequent clouds. SAR is crucial for studying geohazards as it allows for precise detection and measurement of ground movement. Scientists can monitor surface deformations like landslides, subsidence, and volcanic activity by analyzing SAR images over time. SAR's ability to penetrate vegetation is useful for monitoring agriculture, land cover changes, and forest management. It can also detect changes in topography, monitor water resources, and support disaster management efforts like flood mapping and landslide detection (Amitrano et al, 2021; https://www.earthdata.nasa.gov).

2.5.1. Radar remote sensing

Radar remote sensing is a technique for gathering information on the physical and dielectric characteristics of the Earth's surface by using reflected electromagnetic waves. A significant benefit of radar imaging is that it's able to operate independently of the time of day or weather conditions. In this method, microwave pulses are transmitted towards the ground at a specific repetition frequency, which depends on the platform. The roughness and moisture content of the target area affect the intensity and phase of energy reflected back to the radar antenna. The radar antenna creates images of the ground by gathering backscattered radiation. This imaging system is known as side-looking aperture radar because it captures images in a side-looking and forward-moving manner (https://www.earthdata.nasa.gov). Synthetic aperture radar (SAR) is a technique developed in the late 20th century to reduce the size of radar satellites' antennas. It achieves this by utilizing multiple looks at the same ground target.

Sentinel-1 (S-1) is a SAR (Synthetic Aperture Radar) system that operates using C-band and is different from optical systems like Sentinel-2 (S-2). One key distinction is that S-1 is an active system, meaning it doesn't rely on solar radiation. Rather than emitting conventional light, it produces electromagnetic microwave pulses with a wavelength of 5.6 cm to illuminate a targeted area on the Earth's surface. It subsequently receives the signals reflected from objects within this illuminated region. Understanding the disparities in SAR imaging geometry compared to optical sensors is essential for grasping the system's capabilities and limitations, as they are determined by technical specifications (Höser, 2018; Cîmpianu, et al., 2021; ESA, 2018a). understanding the imaging geometry differences between SAR systems and optical sensors is crucial for effectively utilizing each system's capabilities and considering their limitations in various applications presents in Figure 1.

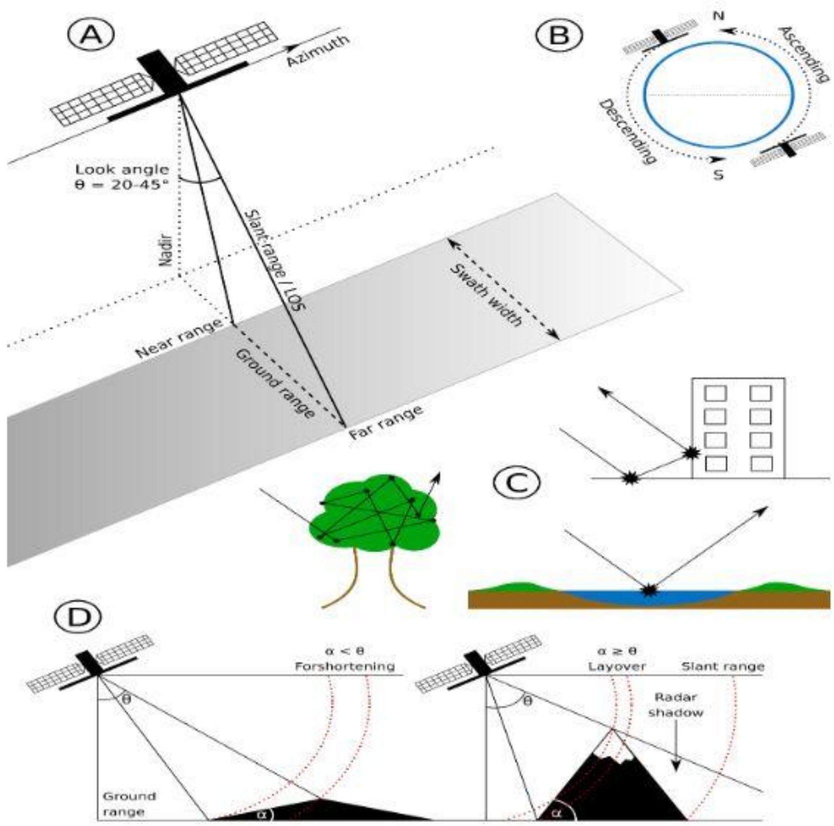

Figure 1: Fundamental sensing geometry, radar sensor scattering, and geometric impacts. **(A)** The side-looking sensing geometry results in the geometric effects shown in **(D)**, where the angle α represents the slope angle. If α is less than θ, the globe appears shortened in the slant range, a phenomenon known as foreshortening**.**If α is less than or equal to θ, the top of the slope appears to be located in front of the foot of the slope in the slant range, a phenomenon known as layover. **(B)** explains the orbit directions, and **(C)** illustrates the typical scattering behaviors of the three principal surface classes, with the arrow indicating the direction of the electromagnetic radiation

from the sensor and its reflection on these surfaces, either towards or away from the sensor which presents in Figure 2. Source: (Höser, 2018).

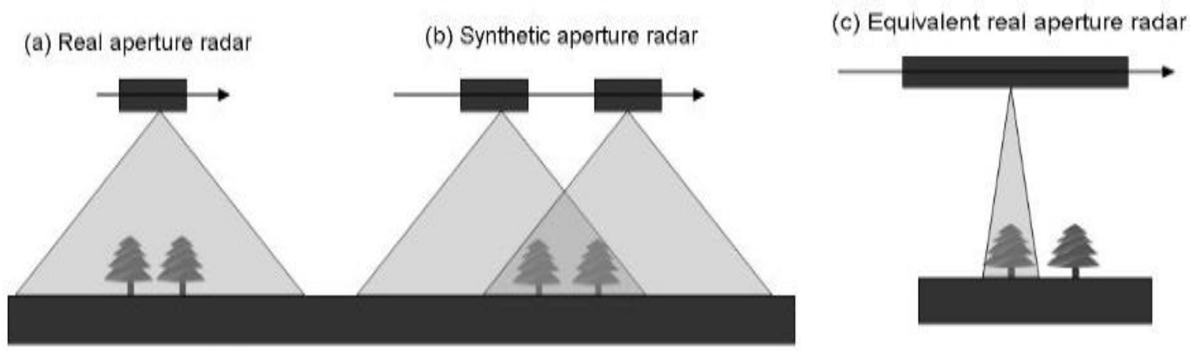

Figure 2. a) Real aperture antenna, (b) Synthetic aperture antenna created by combining information from many pulses and (c) a real aperture antenna that is equivalent to the synthetic aperture antenna. Source: (Agram, 2010).

2.5.2. Persistent scatterer InSAR

PS-InSAR is an advanced multi-temporal interferometric Synthetic Aperture Radar (SAR) technique. It is employed extensively in ground deformation analysis and is capable of detecting and measuring ground displacement with a precision that often reaches the millimeter scale (Nassir, 2019; Natnael and Solomon, 2023). Persistent Scatterer InSAR (PS-InSAR) is indeed an enhancement of traditional InSAR methods, designed specifically to tackle the challenges of temporal decorrelation and atmospheric disturbances, which often hinder accurate remote sensing. The process revolves around the analysis of coherent backscattered signals from a series of multi-temporal Synthetic Aperture Radar (SAR) images – typically a minimum of 15 is required. This method identifies and monitors the signal from uniquely reflective and electromagnetically stable features on the ground known as Permanent Scatterers (PS). The Persistent Scatterer InSAR (PS-InSAR) technique involves analyzing the phase information from at least two Single Look Complex (SLC) SAR images, which are acquired from the same geographic location but at different times. By pairing these images to form an interferogram, the technique allows for the extraction of data regarding ground motion or deformation (Bouchra, et al., 2020).

CHAPTER THREE

3. Materials and methods

3.1 Study area description

The study was conducted at Dessie city, which is a vibrant town. It is located in the Amhara Regional State, northeastern part of Ethiopia, specifically in the South Wollo Zone, is located approximately 400 km north of the capital city of Ethiopia. The journey from Addis Ababa to Dessie typically takes around 6-7 hours by road, depending on the traffic and road conditions. Geographically, the town coordinates found between 39º37'5″−39º41'15″ E longitude and 11º10'35″−11º10'50″N latitude covering a total area of 8844 ha (88.447km^2) Fig 3.1. The textile industry in Dessie has also flourished, with numerous factories producing high-quality fabrics and garments,

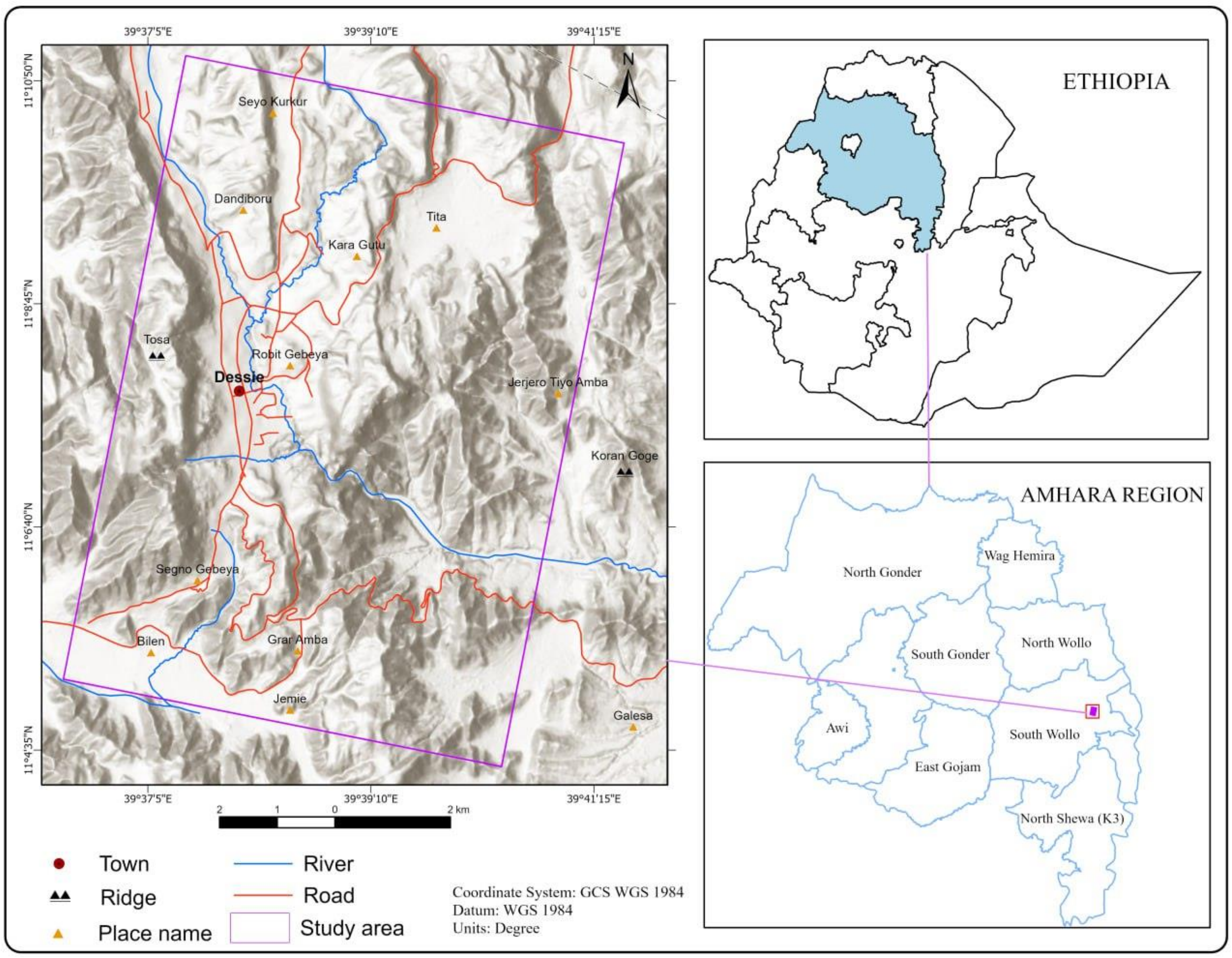

Figure 3.1. Location map of the study area

3.1.1. Topography

Topographically, Dessie City, located in the Ethiopian Highlands, a mountainous region in northeastern Ethiopia, is notable for its geography. The town is situated in a valley surrounded by hills and mountains, with the Great Rift Valley located to the east, offering an attractive setting with breathtaking views. The city itself is located on an elevation range from approximately 1,800 meters to 3,000 m amsl (Fig 3.2).

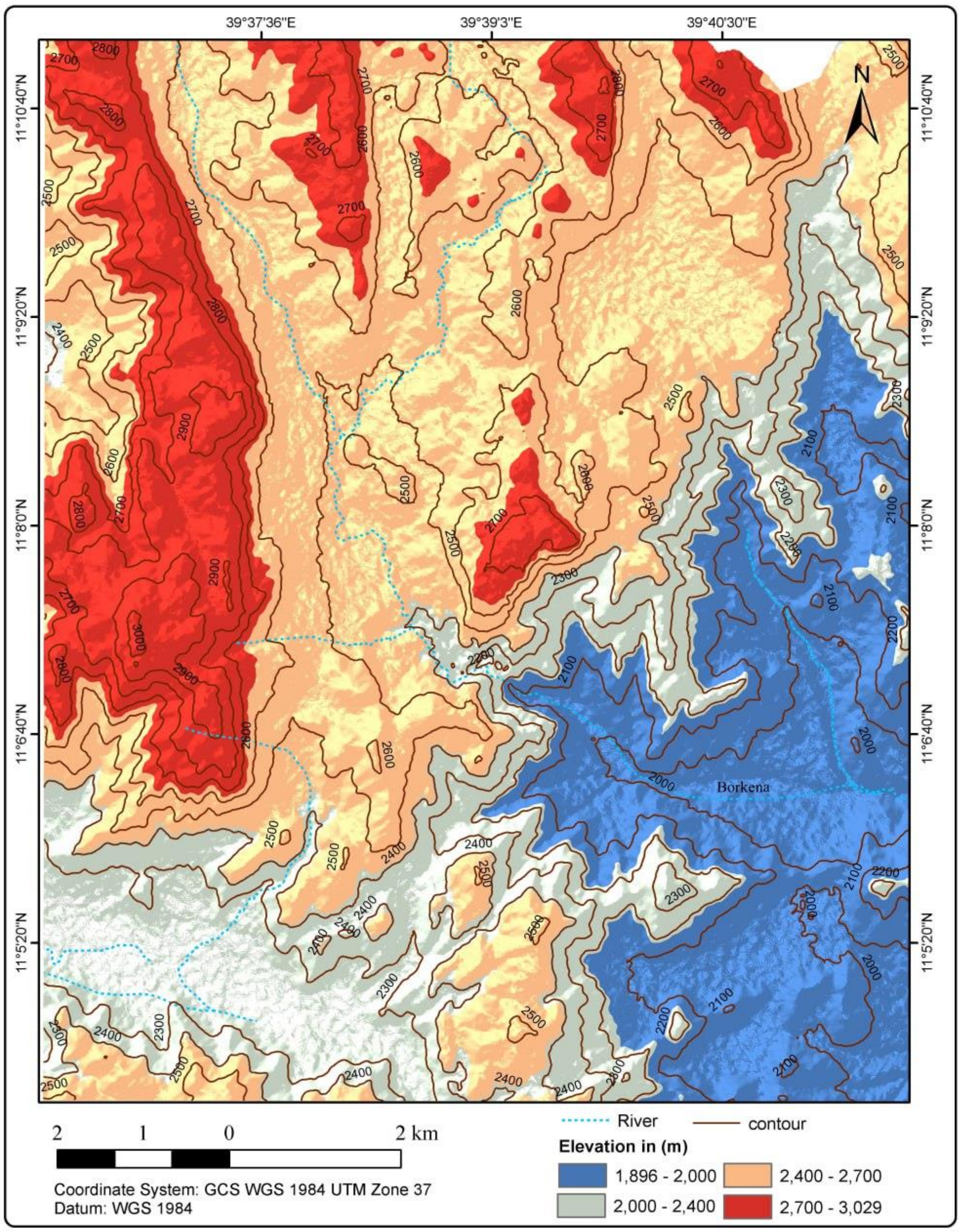

Figure 3.2. Topography map

3.1.2. Drainage pattern

Dessie city exhibits a dendritic drainage pattern. In this pattern, the river channels and streams resemble the branches of a tree, converging at acute angles. The drainage system in Dessie is primarily influenced by the surrounding topography, characterized by hills and mountains. The rivers and streams flow downhill, following the natural slopes and valleys of the area. These water bodies eventually merge and form larger rivers, which flow through or near Dessie city (Fig 3.3). The dendritic drainage pattern is efficient in distributing water and is commonly observed in areas with relatively uniform rock and soil conditions, as found in Dessie.

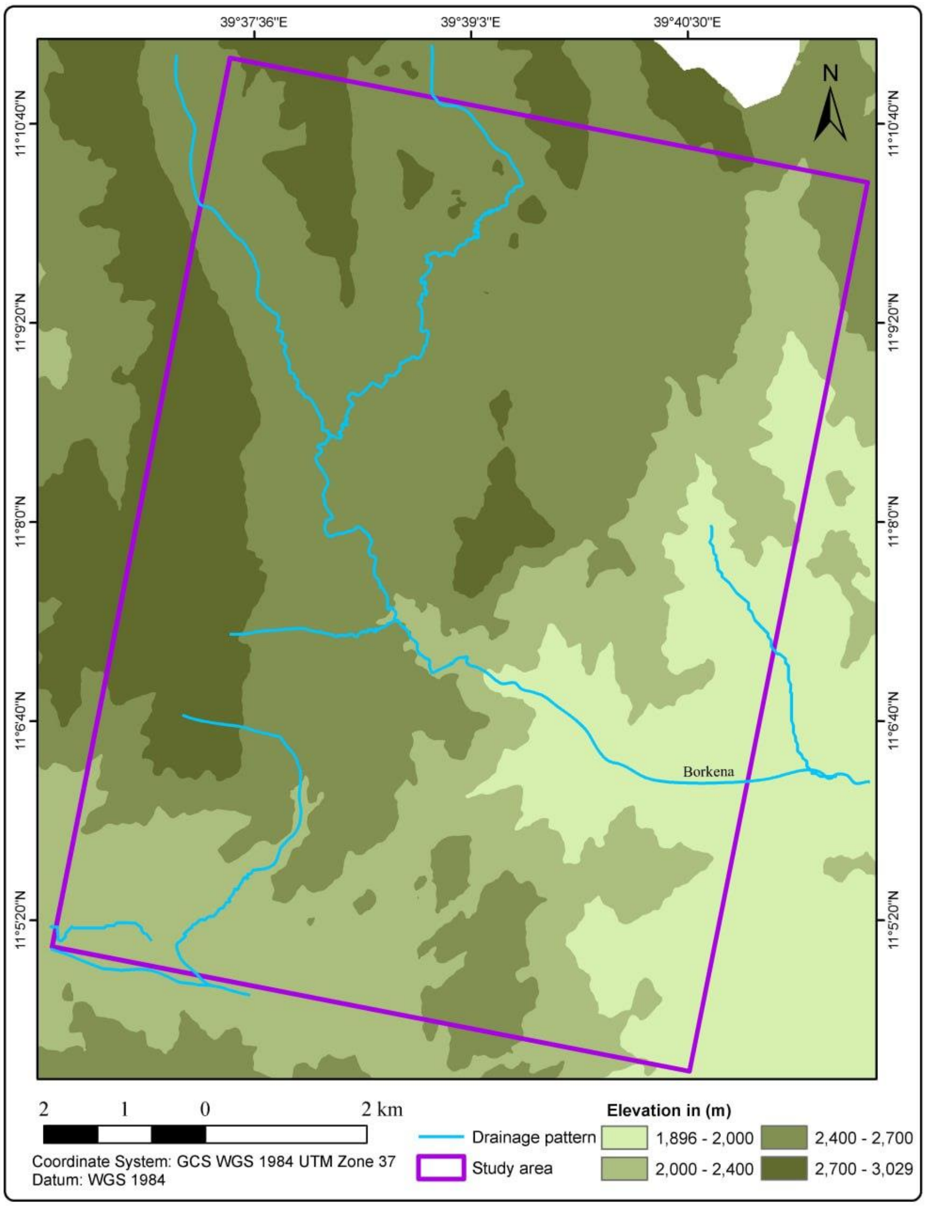

Figure 3.3. Drainage map

3.1.3 Climate

Dessie city practices a subtropical highland climate. The city's elevation contributes to its cooler temperatures compared to lower-lying areas in Ethiopia. The average annual temperature of Dessie fluctuates between 12 °C and 20°C and the average annual rain fall condition from the year 2003 to 2023 in the study area is nearly the same in each year. The study area generally had a high rainfall record in the year 2016, which was about 1400 mm. in the years 2010 and 2019, experience notably high rain falls amounts. In contrast, years such as 2004, 2008 and 2011 observes reduced rainfall levels (Fig. 3.4). on the other hand, the lowest recorded rainfall observed in the year 2015, with an amount of less than 800 mm. The city has incredible dry and wet seasons. The wet season usually takes place from June to September, which helps to support its agricultural activities. Conversely, the dry season extends from October to May, with December and January being the driest months (http://www.ethiomet.gov.et). The climate of Dessie city is generally mild and pleasant, with cooler temperatures compared to many other parts of Ethiopia.

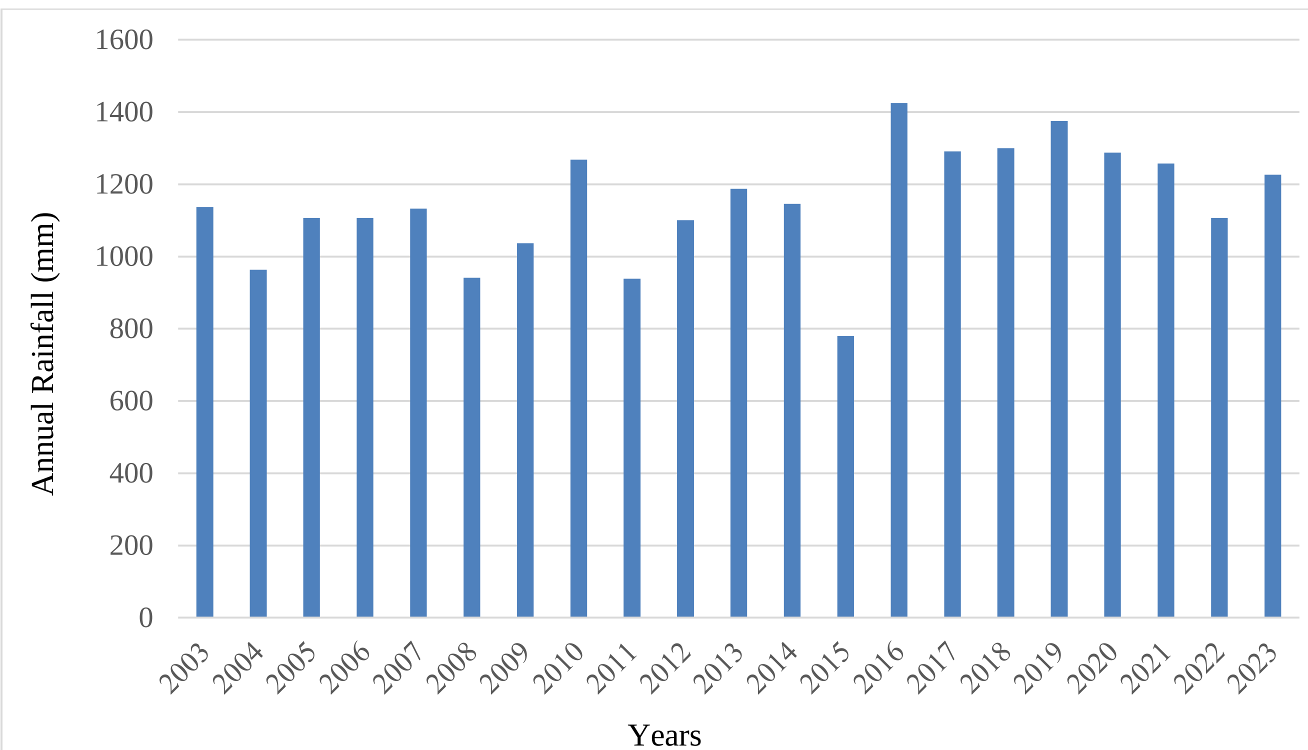

Figure 3.4. Annual rainfall of the study area (2003–2023)

3.1.4. Geology of the area

3.1.4.1. Regional Geology

The study area is part of the northwestern Ethiopian plateau with various geological formations. The Ethiopian area had experienced extensive eruptions of trap successions following the deposition and buildup of Jurassic sediments, mostly in the Oligocene (Abbate et al., 2015). As noted by Abbate et al. (2015), Ethiopia's volcanic regions were divided into five main categories: northern, southern, Somali, Afar, and MER volcanites. The geology of the Dessie area found within the northern Ethiopian highlands. The volcanic phases of the northwestern Ethiopian plateau were classified into three periods, each phase consisting of one or more volcanic formations (Zanettin et al. 1980). These phases are delineated as pre-Oligocene, Oligocene to Miocene, and Miocene to the Pliocene. The oldest rock recorded in the area is Ashangi basalt with approximately 54 million years (Fubelli et al., 2008; Varilova et al., 2015; Tesfaye, 2022). Aiba basalts, wogele Tena rhyolite, Termaber-Guasa formation, Alagi formation, Dessie basalt formation, Termaber-Megezez formation, and Quaternary deposits are the main geological units found in the northwestern Ethiopian plateau (Tesfaye Demissie et al., 2010). The history of geological processes in the region is evident in the presence of diverse lithologies, indicating a long history of tectonic activity, metamorphism, and magmatic processes (Abate et al., 2015; Ayenew, and Barbieri, 2005). This interaction of rocks has led to the formation of intricate geological structures like folds, faults, and shear zones, contributing to the unique and varied terrain of the area.

3.1.4.2. Local Geology of the study area

Dessie is located in the northwestern highlands of Ethiopia along the verge of the southern Afar rift, inside a small graben, and bordered by the steep Tosa and Azewa Gedel fault escarps. Variety lithological units are exposed in the area including basaltic formations, alluvial deposits, colluvial and residual soils. The rock is varying in degree of weathering and strength. The area is intensely affected by fault activity, particularly along the Tossa shield volcanic. Due to this, the geomorphological feature of the area is characterized by deep gorges, grabens, valleys, and ridges.

The geology of the present study area was digitized from the geology map of the region, Google earth and filed observation, and finally mapped (Fig 3.5)

A. Basalt

This lithology unit is highly in the rugged portion of the study area, particularly in the Tossa section. They are characterized by their light black to dark gray weathered and fresh color respectively. They are also characterized by their intensely weathered, fractured, tilted and faulted nature (Fig. 3.5). Basalts with varying from aphanitic to porphyritic textures are observed in the area. Their degree of weathering ranges from highly weathered to low degree of weathering. They constitute varying texture of aphanitic to porphyritic texture. During the on-site investigation, most of the landslides are observed in this lithological units, especially in the Azewa gedel and along Dessie to Kombolcha road section.

B. Alluvial deposit

These are mainly deposited or exposed along Borkena river catchment. The constitutes silt, sand and gravel sized particles. This are deposited on the flat part of the study area in which the sand, silt and gravel particles are transported from the sloppy terrain towards the plain.

C. **Colluvial deposit**

This are deposited on the flat part of the study area in which the sand, silt and gravel particles are transported from the sloppy terrain towards the plain due to gravity. The majority of residential places in Dessie Town are covered with colluvial deposits.

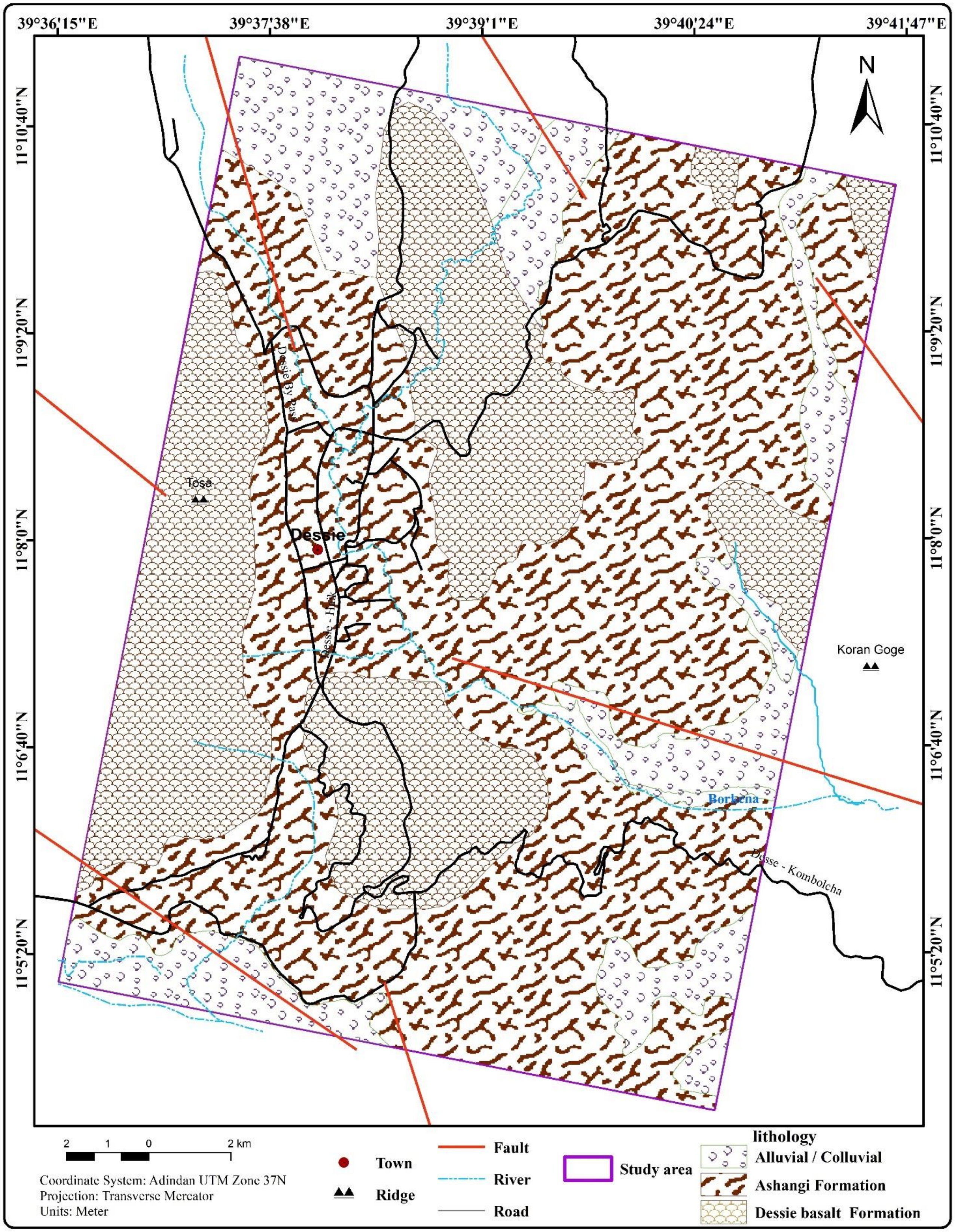

Figure 3.5. Geology map of the study area

3.2 Data and methods

3.2.1. Data and software

The study employed two types of data to analyze its objectives: primary and secondary data. Primary data collected from various sources, comprising geographical data and remote sensing imagery, such as Sentinel-1 images. These satellite images were downloaded freely from ESA websites (https://www.earthdata.nasa.gov/). Sentinel-1 is a sophisticated satellite project created by the European Space Agency (ESA) for the Copernicus program. It has a dual-polarization C-band Synthetic Aperture Radar (SAR) system that allows it to take high-resolution pictures of the Earth's surface in any weather or lighting. Ground verification points were collected using handheld GPS devices and/or Kobo collectors. The Digital Elevation Data (DEM) with a resolution of 12.5 m obtained from the Alaska Satellite Facility. To demonstrate existing area deformation, photographs and field observations was employed. Additionally, internet sources, journals, and published or unpublished government institution manuals and reports was also use as secondary data, which are presented in Table 3.1.

Table 3.1. Description of the data used in the study

Data type	Source	Purpose	Format
Sentinel-1	ESA	To obtain Synthetic Aperture Radar (SAR) data from the Sentinel-1 satellite mission	Raster
DEM 12.5 m	Alaska satellite facility	to extract the topography	Raster
LULC, river, road	SSGI	To prepare thematic layer map	Vector
Ground truth data and Google Earth Image	Field surveys, GPS measurements	To collect data for validation and verification of remote sensing analysis	Vector
photos	Field survey	Reference and verification	Raster

Satellite image use and function are vital. Countries like Ethiopia, known for their diverse landscapes and rich natural resources, have been applying satellite imagery and advanced technologies like Sentinel-1 and SAR (Synthetic Aperture Radar) imagery to support various sectors of the economy (Natnael and Solomon, 2023). These satellite images were acquired freely from ESA websites, and these satellite images provide valuable data and insights for sustainable development, disaster management, and environmental monitoring. According to the

European Space Agency, Sentinel- 1's SAR imagery is particularly useful in disaster management as it allows for rapid assessment of affected areas during natural hazards like floods, earthquakes, and wildfires. the advantages of Sentinel-1 in terms of its high revisit time, which allows for frequent monitoring of landslide-prone areas, enabling the detection of subtle ground movements.

3.2.2 PS InSAR

The field of remote sensing has been revolutionized by the implementation of Satellite Interferometric Synthetic Aperture Radar (InSAR) techniques, facilitating accurate and extensive assessments of ground deformation across vast regions (Zhong, et al 2007). SAR (Synthetic Aperture Radar) images comprise data related to the reflection of radar signals from the surface of the Earth's. The captured images provide valuable insights into the backscattering characteristics exhibited by different objects and terrains (Arsenios et al 2022). The dataset generally comprises of data points related to intensity values, polarization, and spatial resolution, which will be utilized to derive a diverse array of geophysical and environmental parameters.

As the study conducted by (Aswathi et al 2022) Persistent Scatterer InSAR (PSInSAR) methods have gained popularity for their ability to monitor ground deformation at a high spatial density. PSInSAR focuses on identifying and tracking the movement of individual stable targets, known as persistent scatterers, over multiple satellite acquisitions. Persistent Scatterer Interferometric Synthetic Aperture Radar (PS-InSAR) is a sophisticated technique was employed for the examination of specific targets, with a particular focus on monitoring ground displacements such as landslides. The fundamental idea behind DInSAR techniques is to regularly observe and track changes in a specific area over time. By comparing SAR images taken on different dates, a series of differential interferograms is will be created, providing valuable information about the interferometric phase and the effectiveness of PSInSAR in detecting millimeter-level ground displacement, making it an essential tool for monitoring infrastructure stability, land subsidence, and geological hazards (Bouchra et al., 2020).

For the purpose of this study, the InSAR interferometry technique was employed to detect and map landslides using Sentinel 1 data in Dessie City and its surrounding areas. The persistent scatterer interferometry technique will be employed in this study to identify instances of landslide-related deformation in the specified region. Both ascending and descending Sentinel-1 images were utilized to detect surface deformation within the study areas. A total of 290 single-look complex (SLC) images from the Sentinel-1A satellite will be employed for this purpose. These images will be acquired in interferometry wide swath mode (IW) with VV polarization and descending direction spanning from 2018 to 2023. To process the multitemporal synthetic aperture radar (SAR) and InSAR data analysis, the SLC images was registered as master and slave in SARPROZ software, which is specifically designed for this purpose. SARPROZ supports a wide range of satellite formats and imaging modes. Therefore, the use of single-look complex (SLC) data is essential for this analysis (Nassir, 2019).

Interferograms are an essential tool in geodetic studies created through interferometric synthetic aperture radar (InSAR) technology. These images reveal ground deformations and topographic alterations by comparing the interference pattern between two or more radar images acquired at different times over the same area (Berardino et al., 2002; Hanssen, 2001). Sentinel 1A SAR imagery was used to determine time series of average ground settlement rate and vertical line of sight deformation (LOS). To achieve a positive result, PSInSAR requires 15 to 20 acquisitions. A total of 29 images taken between January 2018 to December 2023 were used. The images were taken along the descending orbit. The exact orbits were retrieved by the software for each image SLC (single look complex) images are registered along with single pattern capture. Temporal and spatial decorrelation effects were significantly reduced by the reference image selected by the software (Andinet et al., 2021; Ferretti et al., 2001). interferograms were created from orbital data and an external digital elevation model (DEM) was use to remove flat soil influenced by topography.

When analyzing interferograms, it is important to extract quantitative information about elements such as phase difference, deformations, or terrain changes. Typically, quantifying the deformation of interferograms involves linking fringe patterns (in terms of phase) to actual displacements on the substrate (Andinet et al., 2021, Berardino et al., 2002; Ferretti et al., 2001). This relationship typically includes the wavelength of the radar, the direction of the line of sight, and the geometry of the interferometer system. The phase difference of the interferogram can be determined from:

$$\text{Deformation (mm)} = (\lambda \times \text{Phase Difference (rad)}) / (4\pi \times \text{LOS}) \quad (2)$$

where Radar Wavelength (λ), Phase difference is 2π, LOS is (Line-of-Sight Displacement Factor or for simplicity, assuming LOS displacement in the direction of radar signal)

3.2.3. Landslide triggering factors (zonation)

Environmental factors comprise a dataset anticipated to influence landslide occurrences and serve as causal elements in forecasting future landslides (Mengistu et.al., 2019). Slope angle, lithology, aspect, elevation, and land use and land cover (LULC), rainfall, distance to main roads, and distance to rivers are integral to the analysis of the triggering factor map (Addis, 2023: Korma, 2022). Slope angle, aspect, and elevation were derived from SRTM DEM data at a resolution of 12.5 meters, while other vector datasets were processed using ArcGIS. The lithology layer was obtained from the Geological Survey of Ethiopia at a scale of 1:25,000 and supplemented by field observations conducted during the study. Subsequently, all vector maps were converted into raster format for further examination. The specifics of various triggering factor layers and their respective data source are detailed present in Table 3.2.

Table 3.2 Details of triggering layers with data type and source

Triggering factors	Data	Type	Source
Elevation	SRTM DEM	12.5 m resolution	Alaska satellite facility
Slope	SRTM DEM	12.5 m resolution	Alaska satellite facility
Aspect	SRTM DEM	12.5 m resolution	Alaska satellite facility
LULC	Aerial photo	15 m vector	SSGI
Distance to road	Vector	Line	SSGI
Distance to river	Vector	Line	SSGI
Lithology	Geology map 1:25000	polygon	Geological Survey of Ethiopia
Rainfall (2003-2023)	GEE platform	Point data	CHIRPS

3.3 Software's, tools and their application

For this study, computer hardware and software were used to collect, prepare, analyze, and generate results. The hardware included a personal computer, handheld GPS, and digital camera. The software used was SARPROZ, a software developed by Dr. Daniele Perissin that is specifically designed for multitemporal synthetic aperture radar (SAR) processing. It was written in Matlab and offered a range of modules for the analysis of SAR and InSAR data. It should be noted that a valid license was required in order to use this software, which provided a comprehensive set of tools for processing and analyzing Sentinel-1 SAR data and generating ground deformation maps using InSAR (PS-InSAR). As commercial software, SARPROZ is known for delivering superior results and accuracy. The processing of optical and SAR images is the intent of the SNAP software. SARPROZ, on the other hand, concentrated only on SAR processing; therefore, its results were more accurate. However, different algorithms are used by each software to process SAR data, resulting in varying outcomes. Our main focus is on InSAR processing. The ArcGIS suite was also used to prepare the study area map, other thematic map and to do the hazard zonation map. It was presented in Table 3.3.

Table 3.3. Software, tools and their applications

Software and Tool	Applications
SARPROZ	For processing Sentinel-1 data and generating interferograms / deformation
ArcGIS suit	Analysis, map Layout and Visualization
GPS	To collect Ground control Point
Google earth pro	For Ground verification
Google earth engine	
Digital camera	To collect field photo

3.4 Methodological workflow

The process for carrying out persistent scatterer InSAR deformation analysis included the use of SARPROZ, a software tool, to process and analyze SAR data effectively. This facilitated the creation of a landslide map using InSAR technology, specifically PS-InSAR. Before processing the SAR images, setting up the data and doing a quick analysis. The initial stage involves importing all the SLC data. SARPROZ software identifies the master image that satisfies the criteria of being acquired under moderate climatic conditions and positioned appropriately such as in the middle of the star graph, considering the perpendicular and temporal baseline. Subsequently, the master and slave images are extracted and aligned through precise orbit and digital elevation model co-registration. The SRTM is automatically downloaded as the default DEM. Immediately following co-registration, generate external DEM heights from sources outside the main PSINSAR processing dataset. In the processing of SAR data, this is essential for precisely adjusting for variation in topography. Land hazard zonation map was assessed using ArcGIS spatial analysis tool and all layers converted to 10 m spatial resolution for weighted overlay. A pair wise comparison matrix with in the AHP model was employed to generate the final landslide hazard zonation map. Through the application of these methods, the research delivered a thorough evaluation and mapping of landslide activity in the study area. A visual overview of the methodology is illustrated in Figure 3.6.

3.5 Model validation

In the study of landslides and their triggering factors, the inventory map is a reference, which is a record or database that lists the locations, attributes and effects of landslides that have happened in a specific area called a landslide inventory. Understanding the incidence, distribution and cause of previous landslides is crucial for evaluating and reducing the dangers associated with them and for better knowing the area (Mersha et.al., 2020). Validation involves comparing the mapped landslides or triggering factors with reference data or ground truth information to determine the level of agreement or discrepancy. There are several ways to evaluate the accuracy of landslide monitoring and mapping. In this study, to validate the landslide monitoring and mapping ground truth data, field observations, satellite imagery, and/or aerial photos of the study area were used to compare the mapped landslides with the actual landslides on the ground. This evaluation methodology aligns with the principles outlined by (Opoku et al., 2024), allowing for a comprehensive assessment of the identified land hazard zonation map based on both the overall data set and landslide hazard inventory data obtained from field observation and previous studies with in the entire validation set. Equation (3)

$$\text{Accuracy} = \frac{\text{Total number of agreement data}}{\text{Total number of validation data}} \times 100 \qquad (3)$$

The validation of the PSI deformation map compares the result with known landslide events, ground truth data, or satellite imagery like Google Earth to visually compare the mapped landslides with the actual landslides. This can help identify discrepancies or inaccuracies in the mapping. To verify the landslide inventory map and landslide triggering factors maps of the study area, Field Verification physically visits the identified landslides and compares them with the mapped boundaries. conduct ground surveys and observations to validate the accuracy, and cross-reference the mapped landslides with documented landslide events (correlate) to ensure consistency and accuracy.

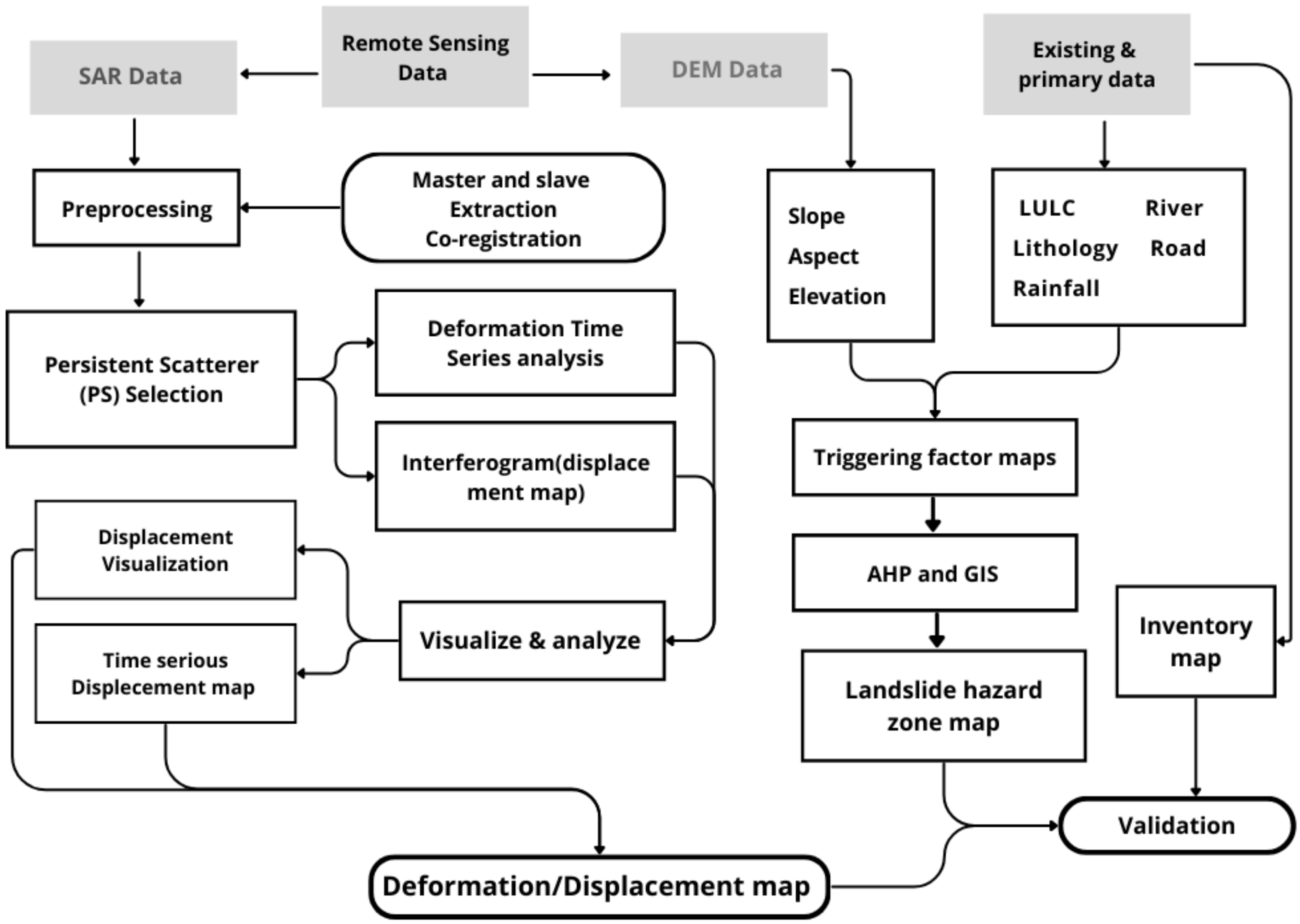

Figure 3.6. Methodology flow chart

CHAPTER FOUR

4. Results and discussion

4.1. Inventory map

Landslide inventory mapping is a vital step in the detection and monitoring of landslides, by locating and recording landslides in a particular location (Mengistu et al., 2019). In this study, a landslide inventory map was made, a total of 15 inventory points for different types of landslides were recorded (Table 4.1), and those inventories appear on Dessie to kombolcha main road, around Menbere tsehay school, Doro mezileya, and Azwa gedel. And most of the inventory was found between the Dessie to kombolcha main road and the Bornena river shown in Fig.4.1.

Table 4.1 landslides inventory point with their latitude and longitude

S/N	Inventory site	Easting	Northing
1	Artificial landfill	570168.75	1227517.33
2	Azwa gedel 1	570773.01	1229137.51
3	Azwa gedel 2	570878.53	1228599.45
4	Jamie sliding 1	570233.85	1227009.12
5	Jamie sliding 2	570297.43	1227247.66
6	Road slide construction	570024.55	1227394.23
7	Rock fall at menbere tsehay	570048.11	1227904.38
8	Menbere tsehay spring and point	569982.87	1228109.82
9	Doro mezileya	570060.30	1229226.93
10	Menbere tsehay point 1	570031.77	1228057.82
11	Harego	571129.96	1227193.73
12	Tosa	567974.57	1229264.45
13	Tita point 1	574351.22	1234443.32
14	Tita point 2	574768.33	1235244.17
15	Dessie adari school	571569.05	1231695.53

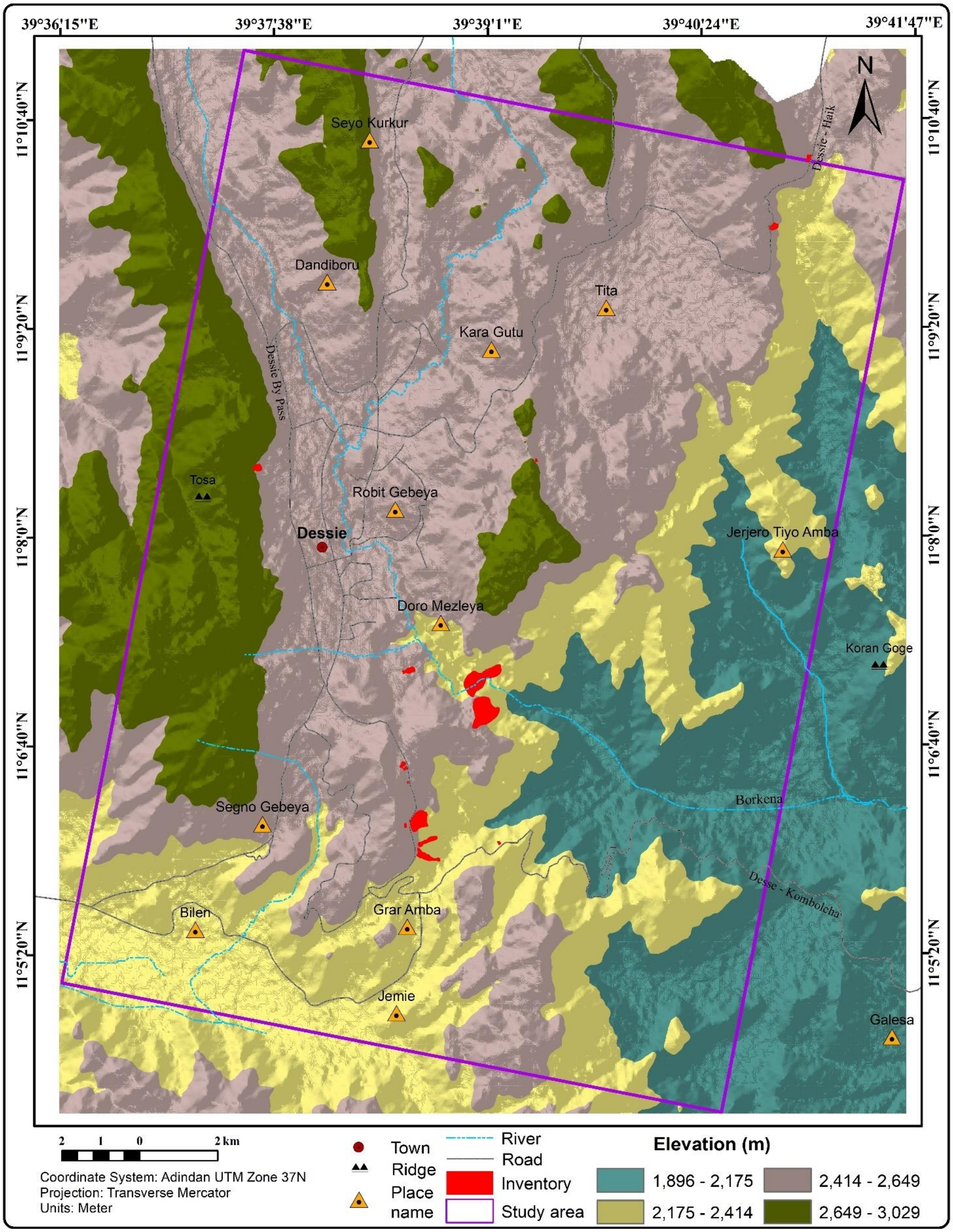

Figure 4.1. Inventory map

4.2. Displacement determination by interferogram and PSInSAR

In the analysis of ground surface deformation and to highlight the key deformation features in the study area, a displacement velocity map is valuable tool derived from interferograms and INSAR time series data. This map effectively highlights significant deformation features in a given area, providing insights into subsidence rates specifically along the Line OF SIGHT (LOS) direction.to generate this displacement velocity map, a single band of SAR data, particularly the C band and Sentinel datasets are utilized. These datasets are carefully evaluated using sophisticated techniques, including persistent scatterer analysis and single interferogram methods. This method is implemented using Sarproz software, a tool renowned for its capabilities in geodetic analysis and deformation monitoring.

Here, for this process, 25 images are used, with the software selecting the default master image Fig 4.2. The study area was manually delineated to concentrate on the city of Dessie, located at Latitude 11.1300 and Longitude 39.6501 within a center 10-kilometre radius. The extracted maters image and the first slave image co-registration through precise orbit Fig. 4.3. The results Reflectivity map and external DEM height generate from default SRTM DEM which is sources outside the main PSINSAR processing dataset Fig 4.4. In the process of estimating APS for accurate results, a series of spatial-temporal filters are employed to minimize discrepancies in the data. Initially, the selection of the First PS-point with a threshold of 0.8 is crucial, as it contributes to obtaining precise APS estimations (Fárová et al., 2019) present in (Fig. 4.5a). Although only a few points meet this strict criterion, they play a significant role in the process, here in this study138 sparse point were satisfy the criteria (Fig. 4.5b.) Following the selection of PS Points, a reference network is formed by connecting these points through Delaunay Triangulation. This step is fundamental in estimating the atmospheric phase screen. Subsequently, a second set of PS-Points is added through sparse points processing to enhance the network's density. The points connected based on Delaunay Triangulation Principles form a Delaunay Network, characterized by a triangular network where the circumcircles of all triangles are empty. The Delaunay Triangulation network is constructed with a minimal number of arcs to ensure lower displacement accuracy. Any arcs exceeding the maximum correlated atmospheric length are eliminated to reduce redundancy in the network. Linear displacement velocities and residual height estimates are excluded, and APS is calculated from the remaining phases using graph inversion. It is crucial to choose a reference point that incorporates the characteristics of both the residual histogram height value and the peak of the estimated velocity histogram at zero

Fig. 4.6. This is to ensure the reference point is on the ground and stable (Bokhari et al., 2023; Qin, 2018) present in Fig. 4.7.b. The quality of the estimated APS is evaluated through temporal coherence analysis of PS Points post-graph inversion and APS removal. This analysis reveals satisfactory results, with most points exhibiting a coherence value above 0.9 this indicates the selected area location is coherent and good measurement reliability (Figures 4.5b,4.7b, and 4.8).

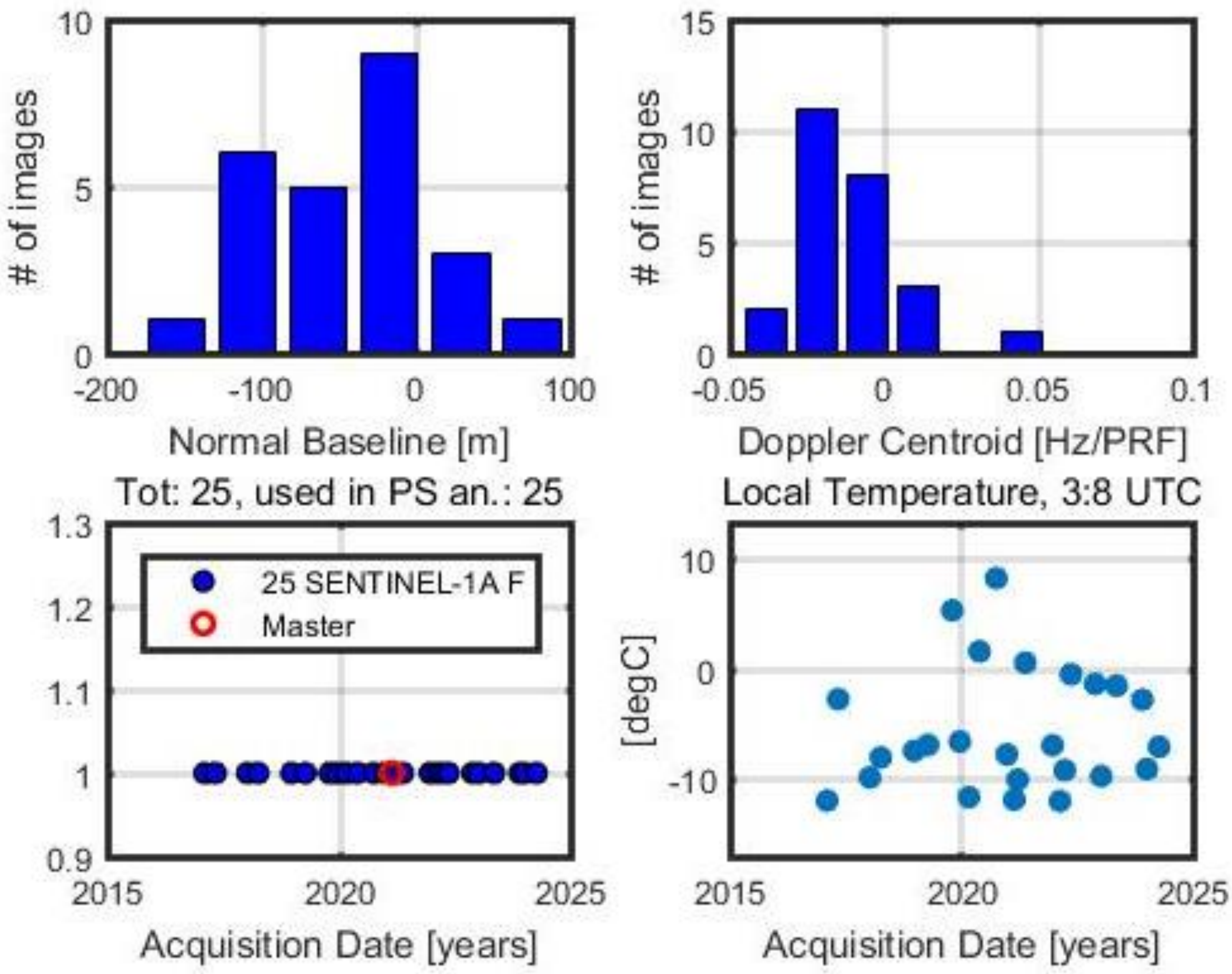

Figure 4.2 SLC dataset statistics

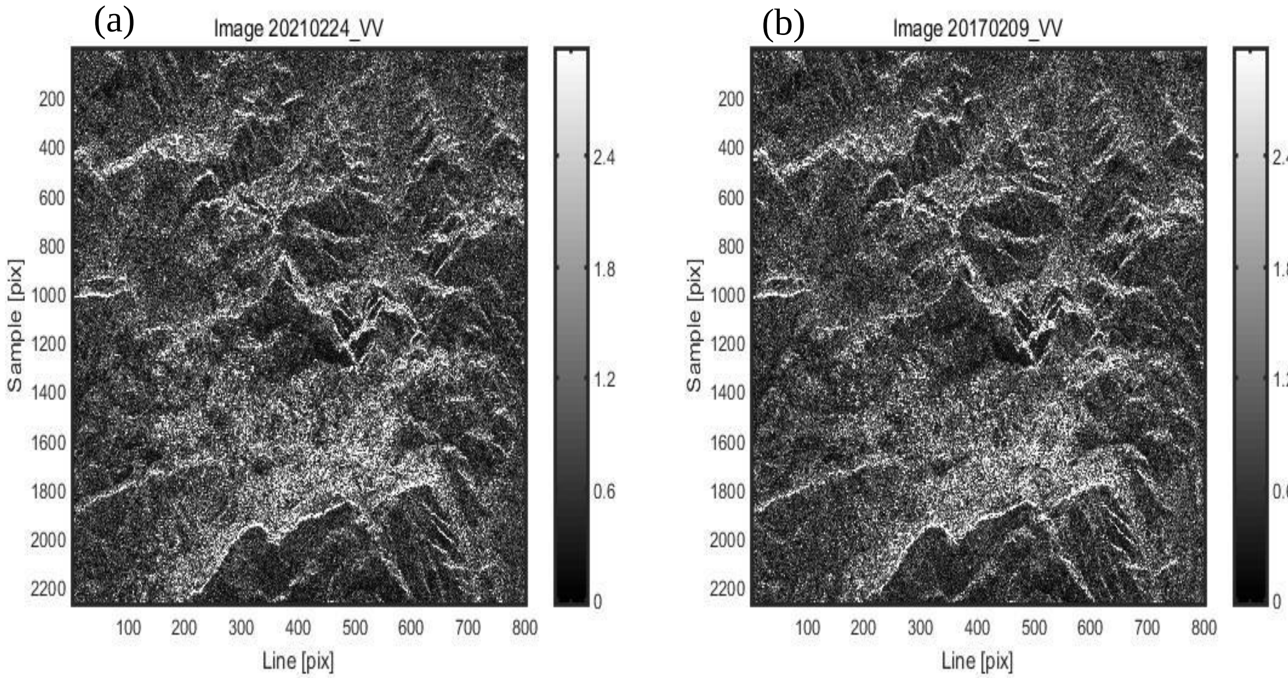

Figure 4.3. Master images extraction (a), and first slave image co-registration (b)

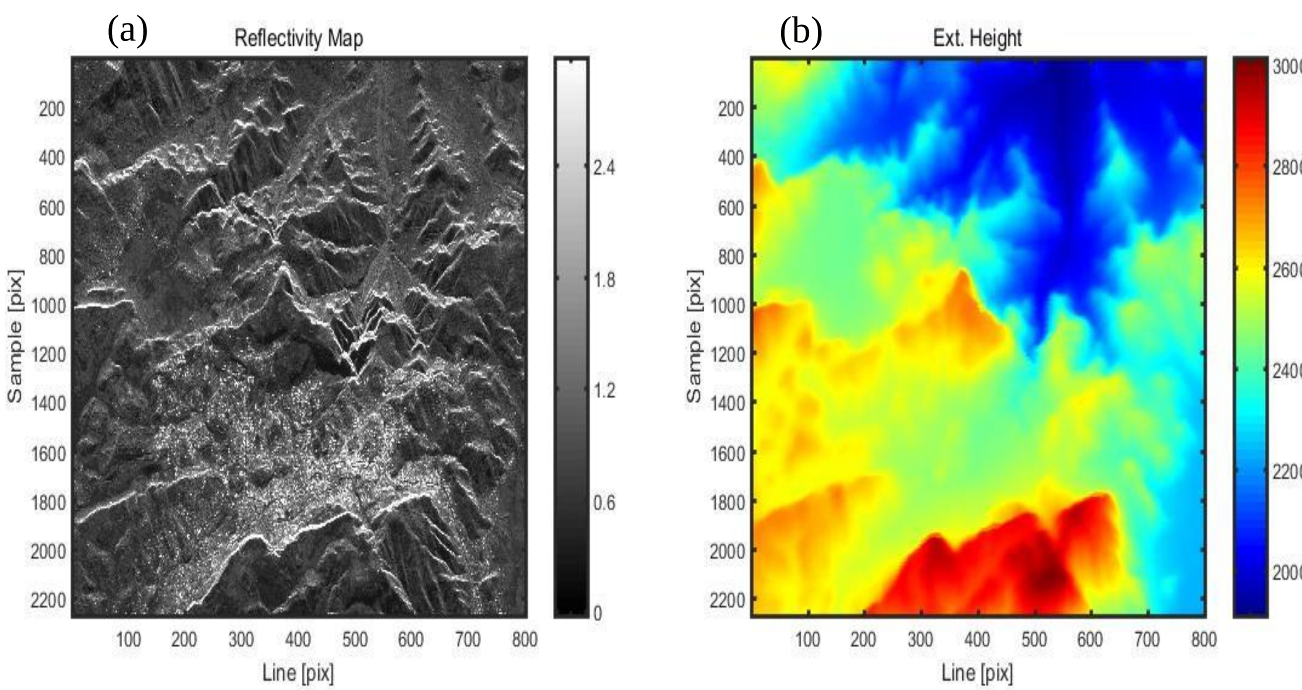

Figure 4.4 Reflectivity map and external DEM height of the study area

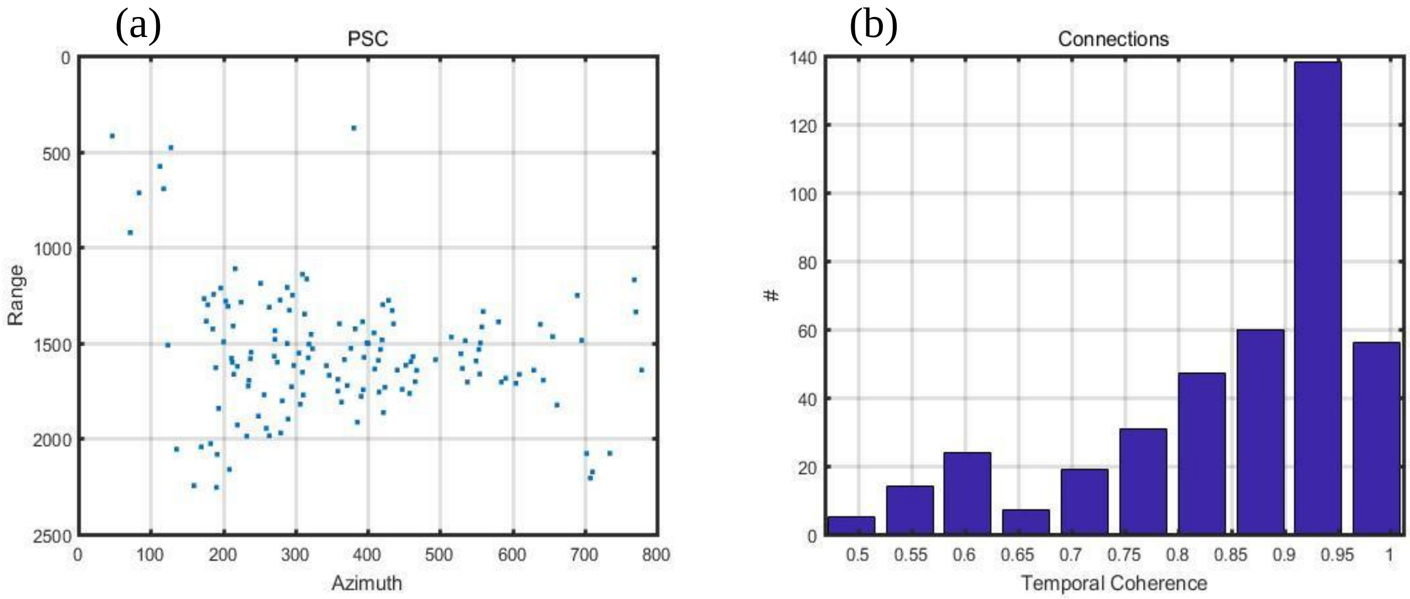

Figure 4.5 Plot of sparse point selection (a) and histogram of graph connection coherence with selected sparse point (b)

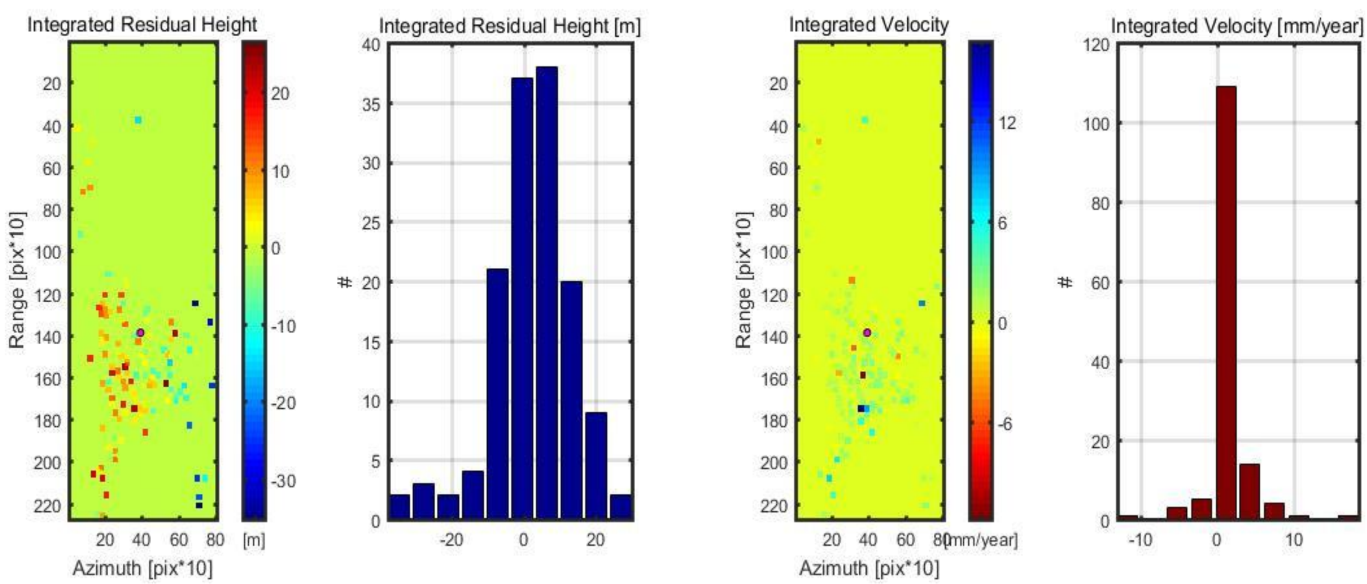

Figure 4.6 Graph and histogram of residual height and velocity histogram

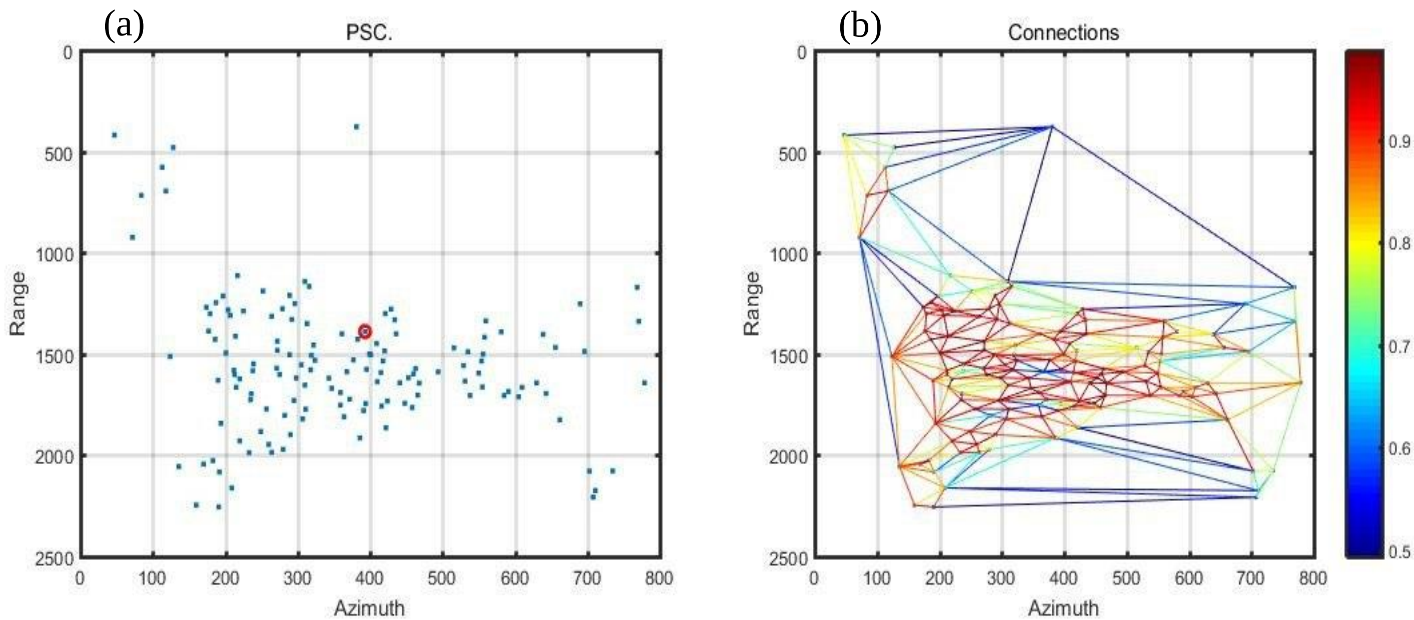

Figure 4.7. sparse point automatic reference points(a) and plot of Delaunay graph connection coherence sparse point automatic reference points(b)

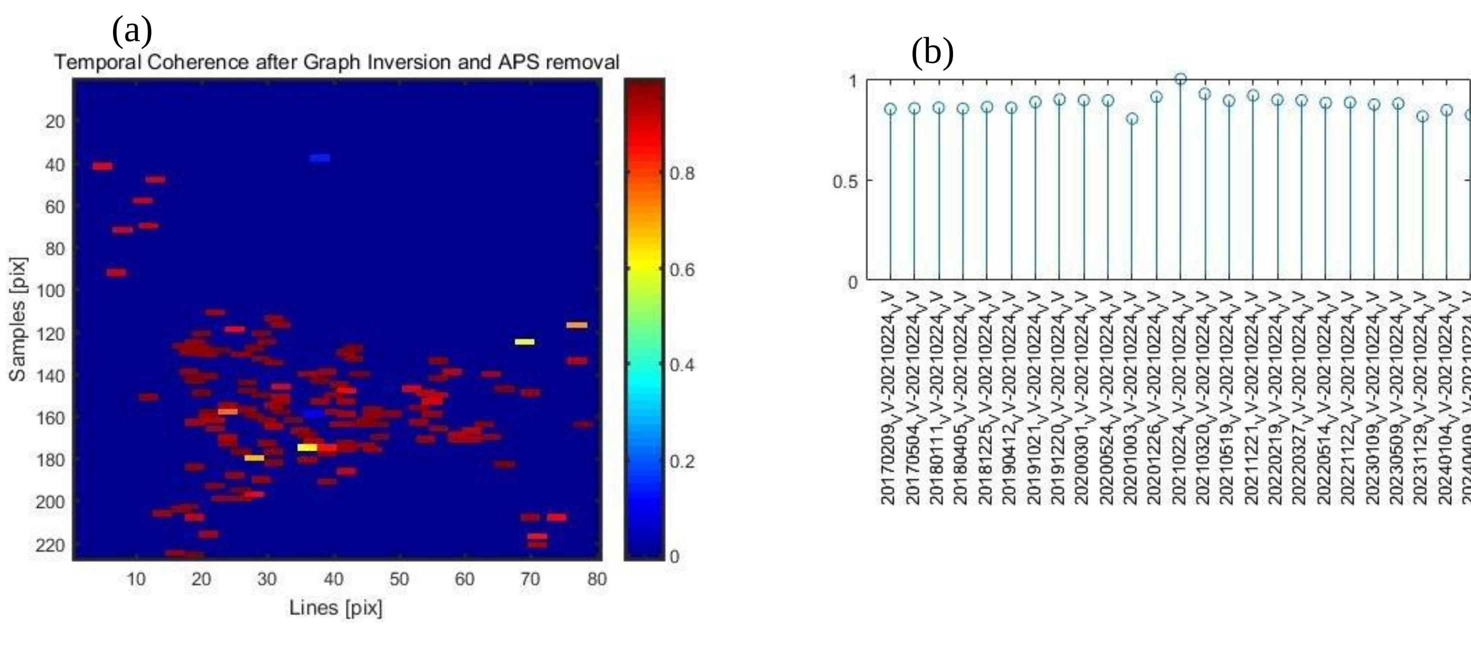

Figure 4.8. Temporal coherence of points after removing the estimated APS(a) and Coherence between each slave date and the master date after removing the estimated APS(b)

4.2.1. Ground displacement by PSInSAR

The Persistent Scatterer Interferometric Synthetic Aperture Radar (PSInSAR) analysis conducted in the Dessie area between 2017 and 2024, significant ground movement patterns have been observed. The study reveals varying degrees of displacement and velocity across the area, as shown in Fig. 4.9. The color scheme used, with red indicating subsidence, blue indicating uplift, and yellow representing stability, helps to visualize the changes effectively. the result shown in terms of vertically (subsidence or uplift) or horizontally, with velocity. Over the period of seven years from 2017 up to 2024, the recorded maximum cumulative displacement was -64.1 mm, while the minimum cumulative displacement was -19.8 mm.

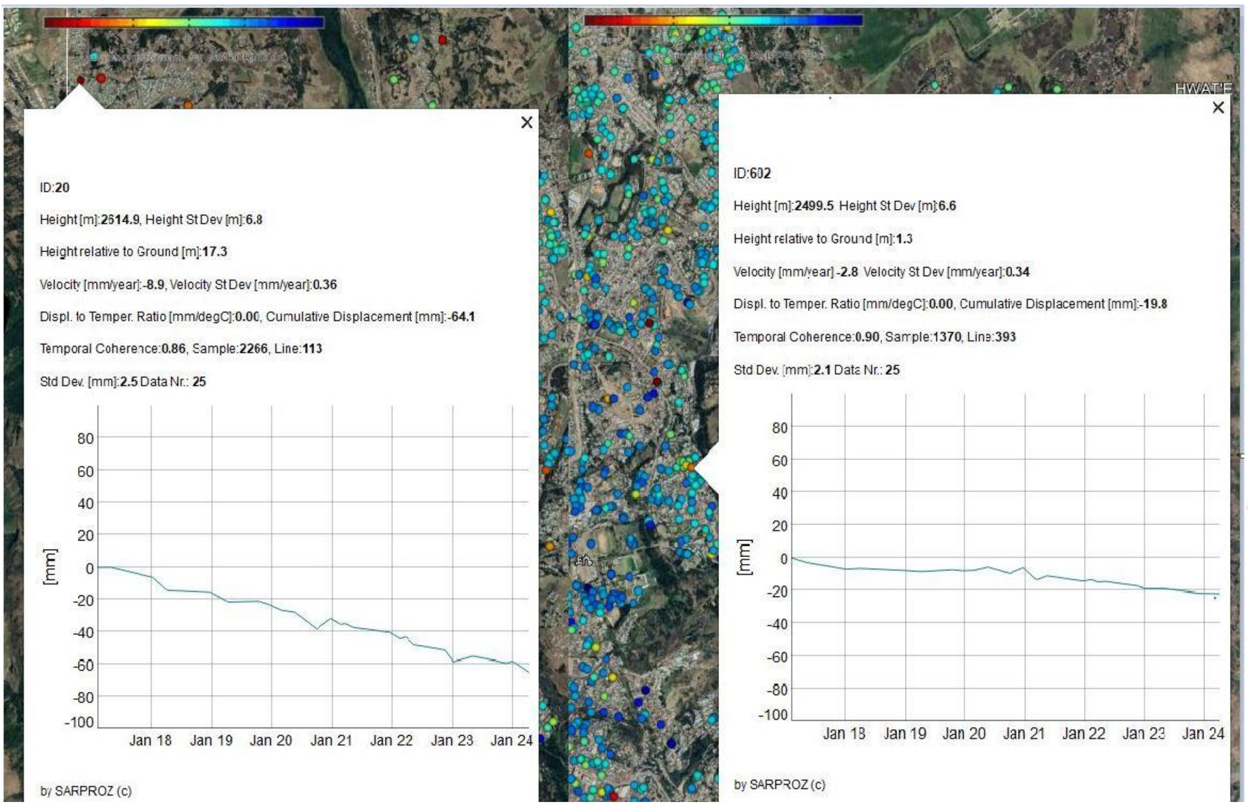

Figure 4.9 PS approach Graph shown maximum and minimum cumulative displacement

In order to provide a clearer illustration of the surface displacement change in Dessie, time series for three different locations are chosen. These locations, which are situated in the central, northwestern, and northeastern parts of the study area aligning with the sliding surface, their respective locality name around Ayteyef, Yohanes Church, Dessie Adari school were carefully chosen based on the landslide inventory map. This deliberate selection allows for a comprehensive understanding of the time evolution of surface displacement in Dessie, capturing the level of movement in different parts of the study area.

4.2.1.1 Test location 1 (around Yohannes church)

In this study, PSI analysis result showed that test location 1 stands out in the study area with the highest cumulative displacement values of –64.1 mm subsidence and a velocity of 0.36 mm per year. This indicates that test location one is the most critical and unstable area in the Dessie presented in Fig 4.10. From 2017 to 2024, the test location1 area's time series study demonstrates an ongoing increase trend which is presented in Fig 4.11. The displacement per year was measured in the following years: 2018, 2019, 2020, 2023, and 2024; the values were –14.2 mm, –21.7 mm, –38.5 mm, –58.6 mm, and –65 mm, in that order. This analysis illustrates a concerning pattern of increasing displacement over the years, indicating significant changes to the local topography.

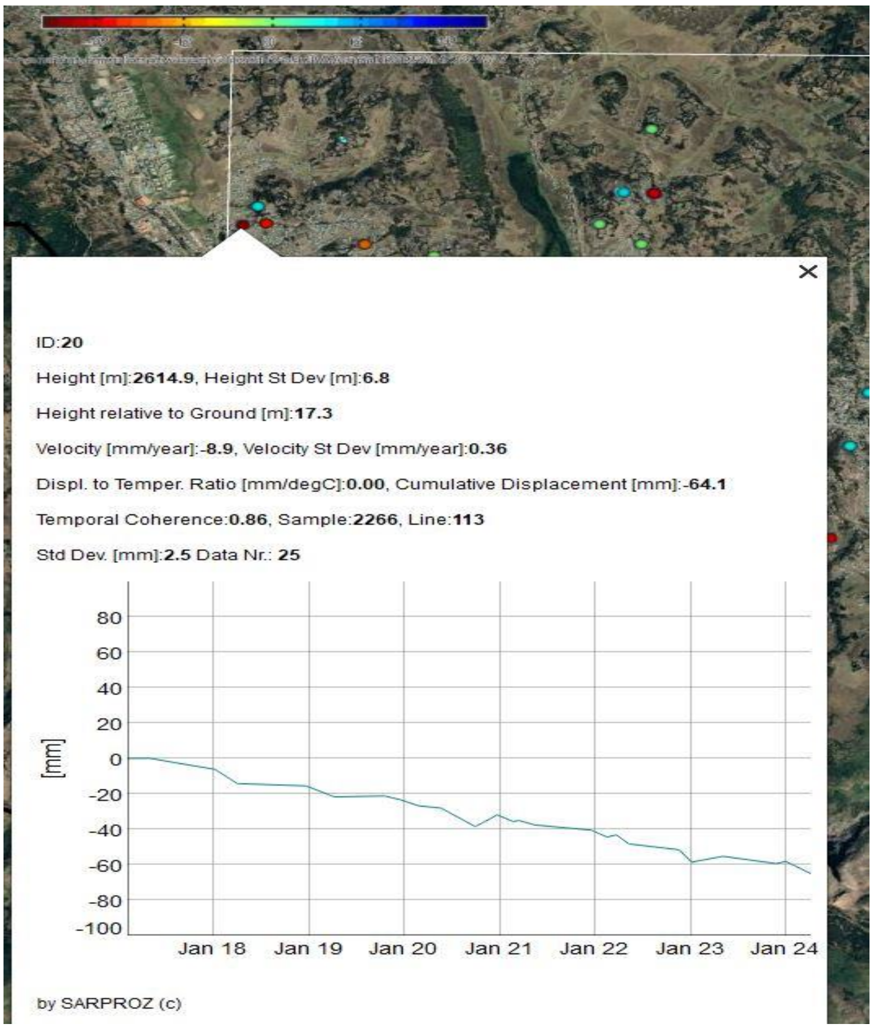

Figure 4.10. Graph shown cumulative displacement and velocity Yohannes church in Dessie.

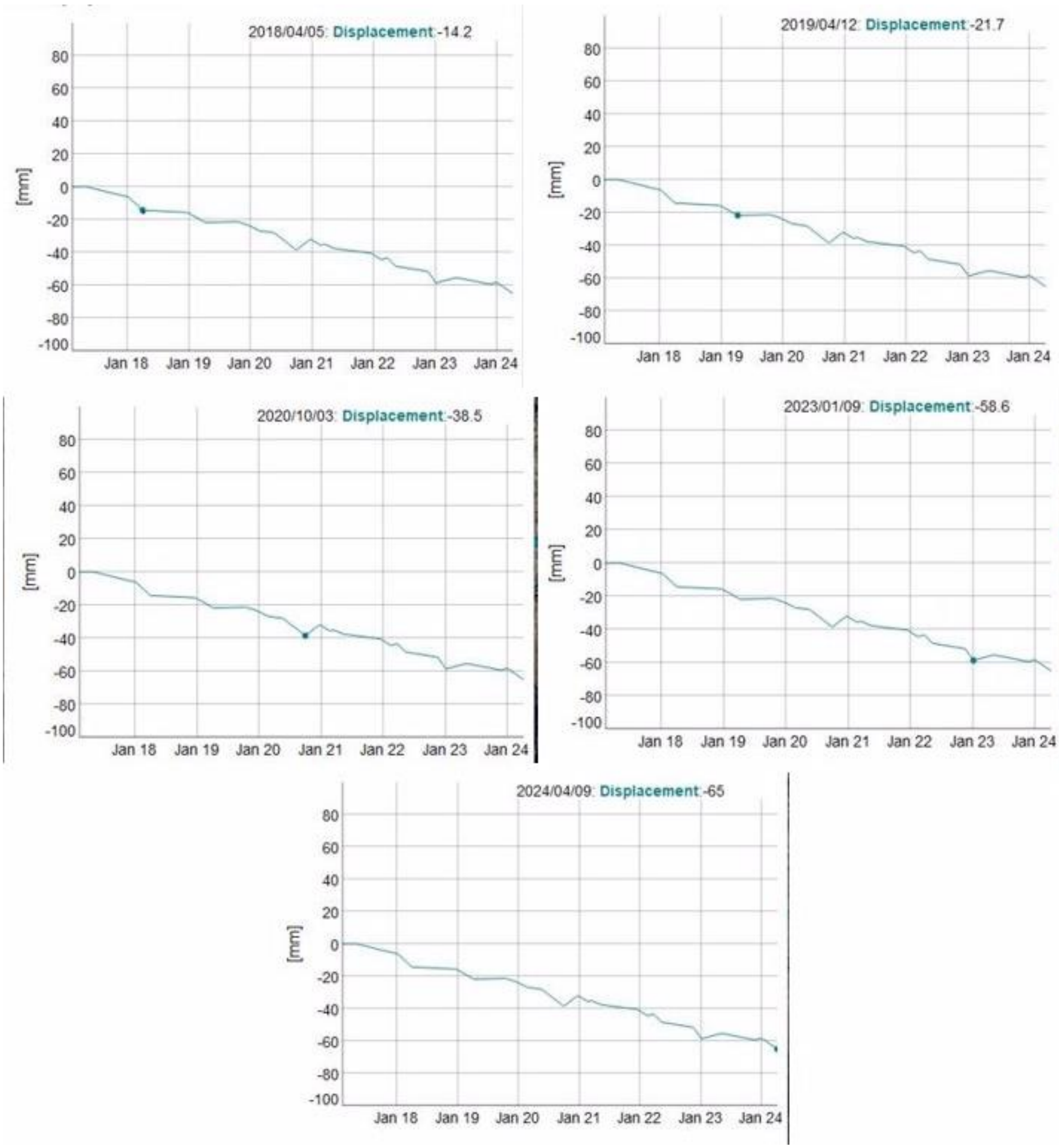

Figure 4.11. Graph shows the displacement time series trend selected PS point during 2017 up to 2024

4.2.1.2. Test location 2 (locality name Ayteyef)

In this work, PSI analysis result showed that test location 2 stands out in the study area with cumulative displacement values of -29.5 mm subsidence and a velocity of 0.38 mm per year. unstable area in the Dessie shown in Fig.4.12. From 2017 to 2024, the test location 2 area's time series study demonstrates an ongoing increase trend which presented in Fig.4.13. The displacement per year was measured in the following years: 2018, 2019, 2020, 2021, 2023, and 2024; the values were –12.4 mm, –16.5 mm, –21.2 mm, –23.5 mm, –25.2mm and –29.3 mm, in that order. This analysis illustrates a concerning pattern of increasing displacement over the years, indicating significant changes to the local topography.

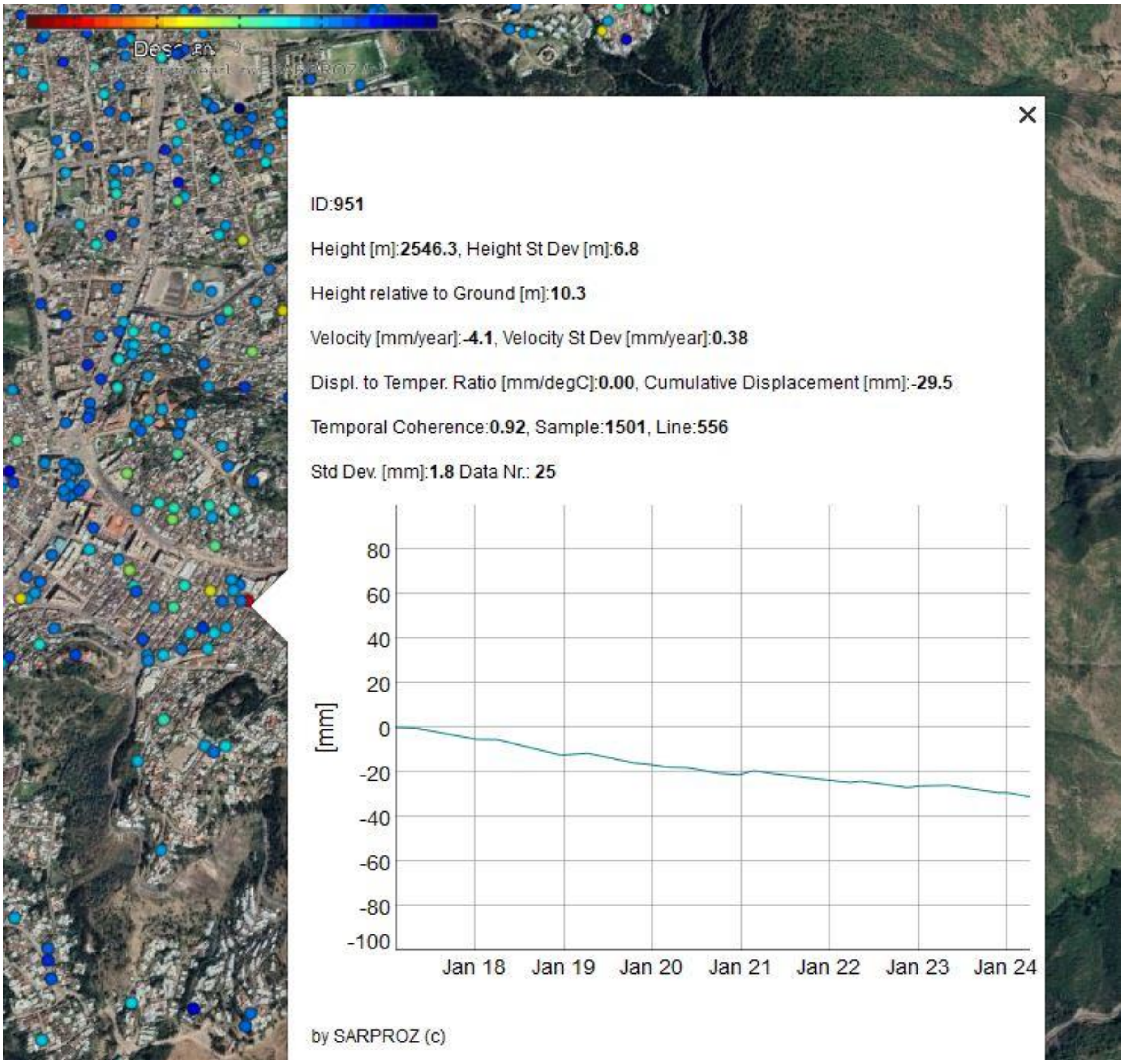

Figure 4.12 Graph shown cumulative displacement and velocity around Ayteyef in Dessie.

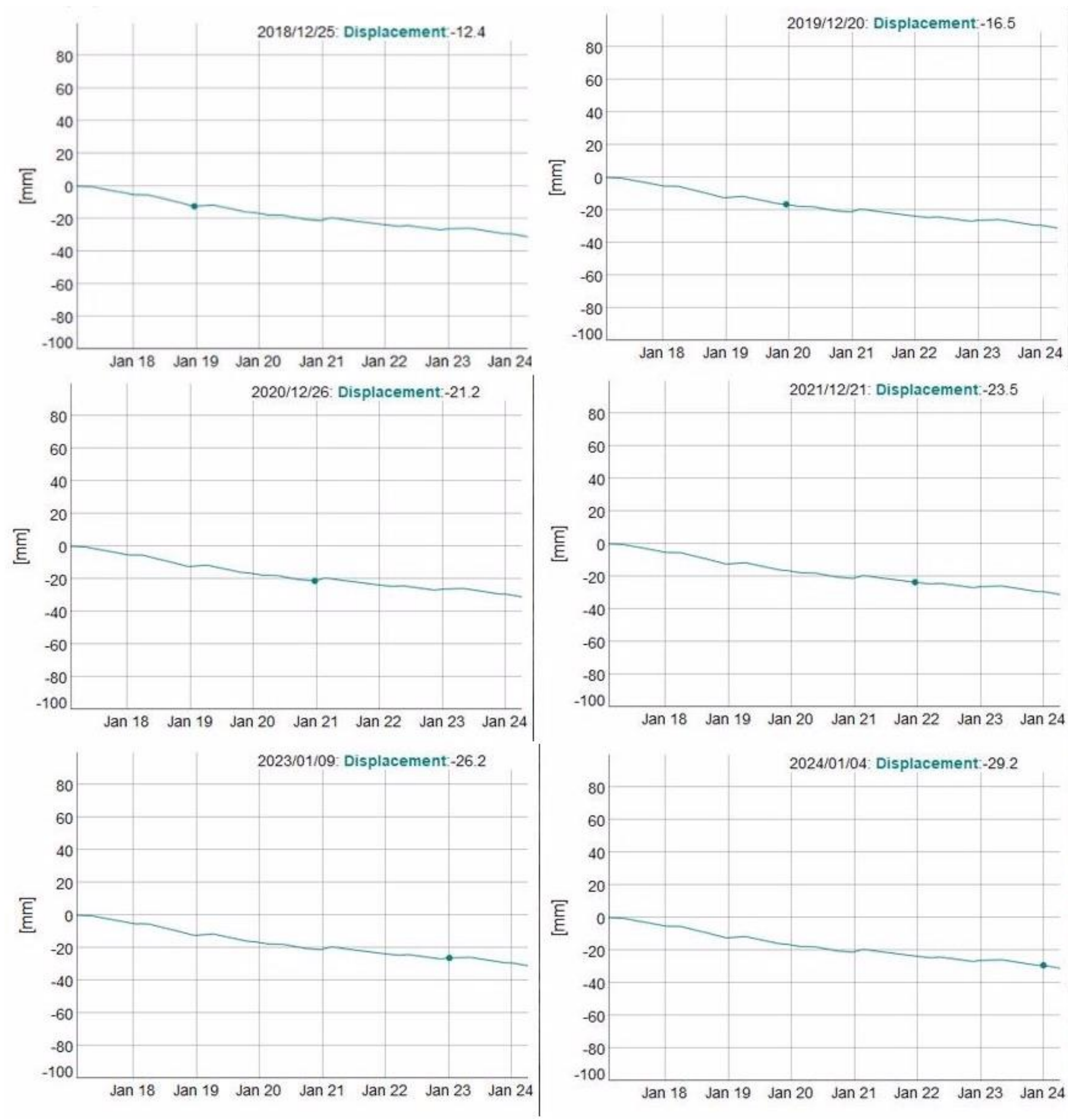

Figure 4.13. Graph shows the displacement time series trend selected PS point during 2018 up to 2024

4.2.1.3 Test location 3 (locality name Dessie Adari school)

In this work, PSI analysis result showed that test location 3 stands out in the study area with cumulative displacement values of -29.6 mm subsidence and a velocity of 0.35 mm per year. unstable area in the Dessie shown in Fig.4.14. From 2017 to 2024, the test location 3 area's time series study demonstrates an ongoing increase subsidence trend which presented in Fig.4.15. The displacement per year was measured in the following years: 2017, 2018, 2019, 2020, 2021,2022, 2023, and 2024; the values were –2 mm, -10.7 mm, –13.8 mm, –15.6 mm, –21.1mm, –24.6mm, -–27.8 and –29 mm, in that order. This analysis illustrates a concerning pattern of increasing displacement which is subsidence over the years, indicating significant changes to the local topography.

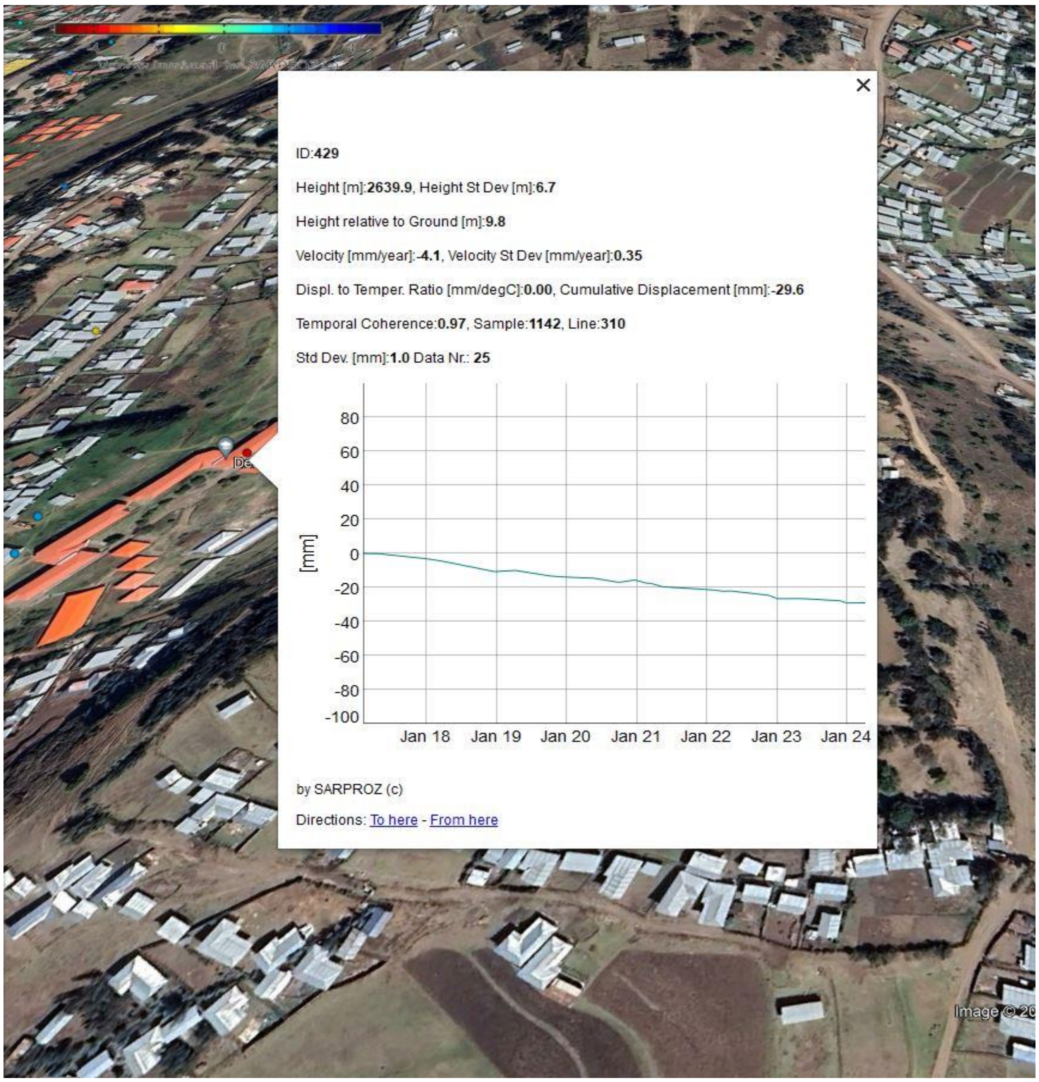

Figure 4.14 Graph shown cumulative displacement around Dessie Adari school in Dessie.

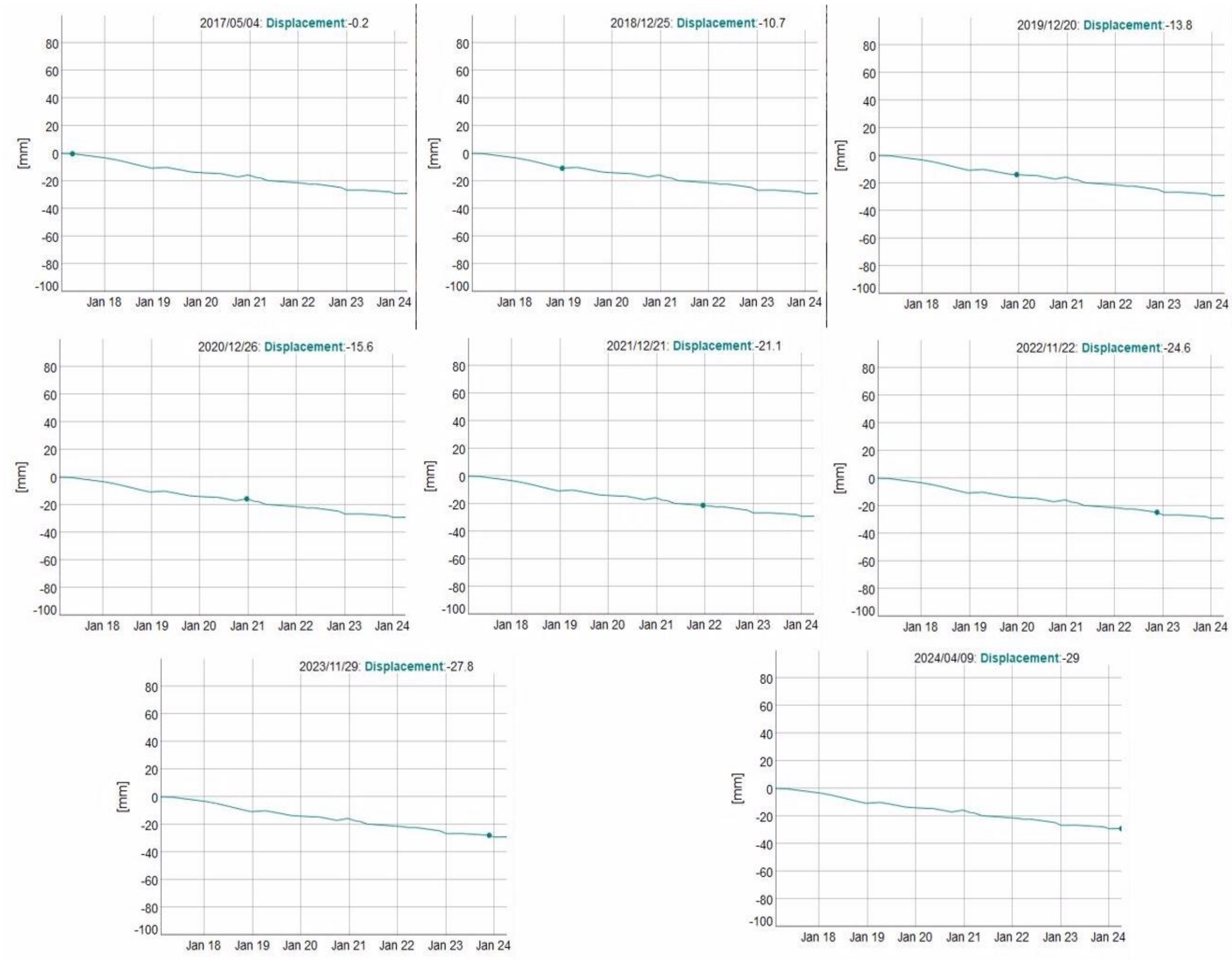

Figure 4.15. Graph shows the displacement time series trend selected PS point during 2017 up to 2024

4.3. Landslide triggering factors

4.3.1 Slope

The slope of the study area ranges from 0° to 75°, Fig. 4.16 a, indicates the slope of the study area categorized in five classes, including flat (0° – 8.82°), gentle (8.83° – 17.3°), steep (17.4° – 26.7°), very steep (26.8° – 37.6°), and very very steep (37.7° – 75°). There is a noticeable correlation between slope and landslides, with steep slopes being more vulnerable to landslides, and conversely, slopes with a flat with a flat angle are less vulnerable to landslide hazards.

4.3.2. Aspect

The aspect map of the study area was classified according to the angles; Flat (-1°−0°), North (0°−22.5°), Northeast (22.5°−67.5°), East (67.5°−112.5°), Southeast (112.5°−157.5°), South (157.5°−202.5°), Southwest (202.5°−247.5°), West (247.5°−292.5°), Northwest (292.5°−337.5°) and North (337.5°−360°) (Fig 4.16 b). The aspect angle of a slope influences the probability of landslides. Slopes facing northern part of the study area receive less sunshine, which increases soil moisture levels and increases the chance of landslides during rainy season. Conversely, because they receive more sunlight, south facing slopes dry out more quickly, which lowers the chance of landslides.

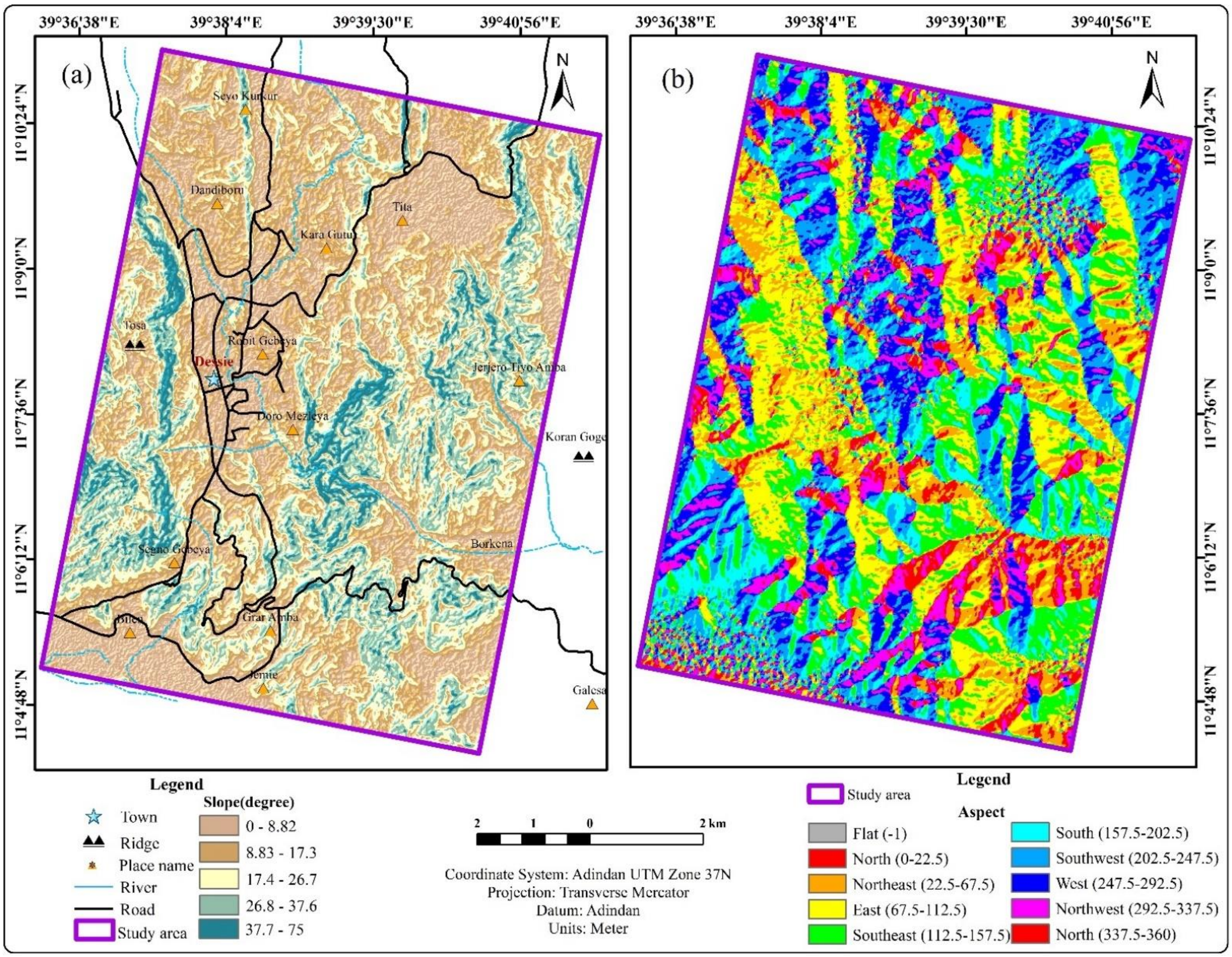

Figure 4.16. Slope map (a), and Aspect map (b)

4.3.3. Elevation

The elevation map of the study area spans from 1930 to 3030 meters above mean sea level, compressing the diverse topographical conditions conducive to landslide occurrences. Fig. 4.17a, provides a comprehensive depiction of elevation distribution in the study area. Hence, the study area has varied topography, and there is a considerable correlation between elevation and landslides. Landslides are frequently more common at higher elevations.

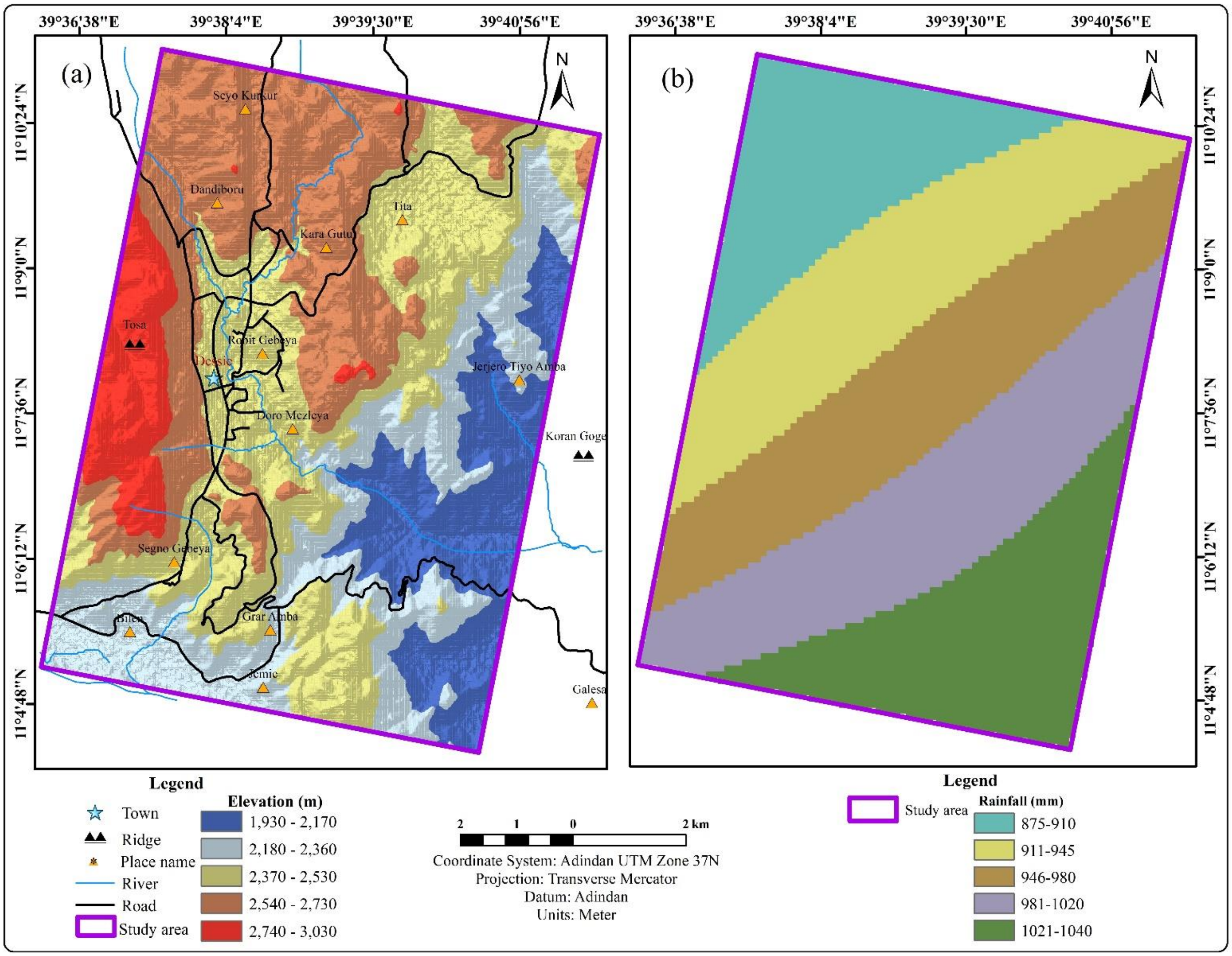

Figure 4.17. Elevation map (a), and Rainfall map (b)

4.3.4. Rainfall

The average annual rainfall in the study area varies between 875 mm and 1040 mm. Fig. 4.17b. The interpolated rainfall data reveals notable spatial disparities in rainfall distribution across the study area. Provides detailed insights to the spatial distribution of rainfall across the study area.

which significantly influence landslide susceptibility during high rainfall intensity in areas with high topography.

4.3.5. Land-use and land-cover

The land-use and land-cover of the study area was classified as five classes: vegetation, built-up area, open area, cultivation land, swampy area and. Cultivation land, which covers 2927.21 ha (33%) of the total study area. Thus, cultivation land in the study area shows highest probability for landslide occurrence in the study area. This is followed by open area 853 ha (10%) of the total study area, and built-up area 2996.8 ha (33.88%) this class also shows reasonable probability for landslide occurrence. Moreover, vegetation covers 2008.42 ha (22.62%), and swamp area swampy area 46.37 ha (0.5%) of the study area show least probability for landslide occurrence. Table 4.2 details of LULC area coverage and its percentage. Fig. 4.18a describe the LULC classification.

Table 4.2 Land-use and land-cover with area coverage

LULC class	Area (ha)	Area (%)
Cultivation land	2927.21	33
Vegetation	2008.42	22.62
Open area	853	10
Built-up	2996.8	33.88
Swampy area	46.37	0.5

4.3.6. Lithology

In the study area, lithological units classified mainly in three which is Dessie Basalt Formation, characterized by dense, hard basaltic rocks with fine-grained textures and columnar jointing, demonstrates low susceptibility to landslides owing to its inherent strength and resistance to weathering and have a large share from the study area. On the other hand, the Ashangi Formation, which cover most area in the study area, composed of sedimentary rocks like sandstones, siltstones, and shales, formed in ancient marine or fluvial environments, exhibits moderate susceptibility to landslides. While sandstones may offer resistance to weathering, the presence shales and siltstones, coupled with factors like bedding planes and lithological heterogeneity, can contribute to localized slope instability, particularly under saturated conditions Fig. 18 b.

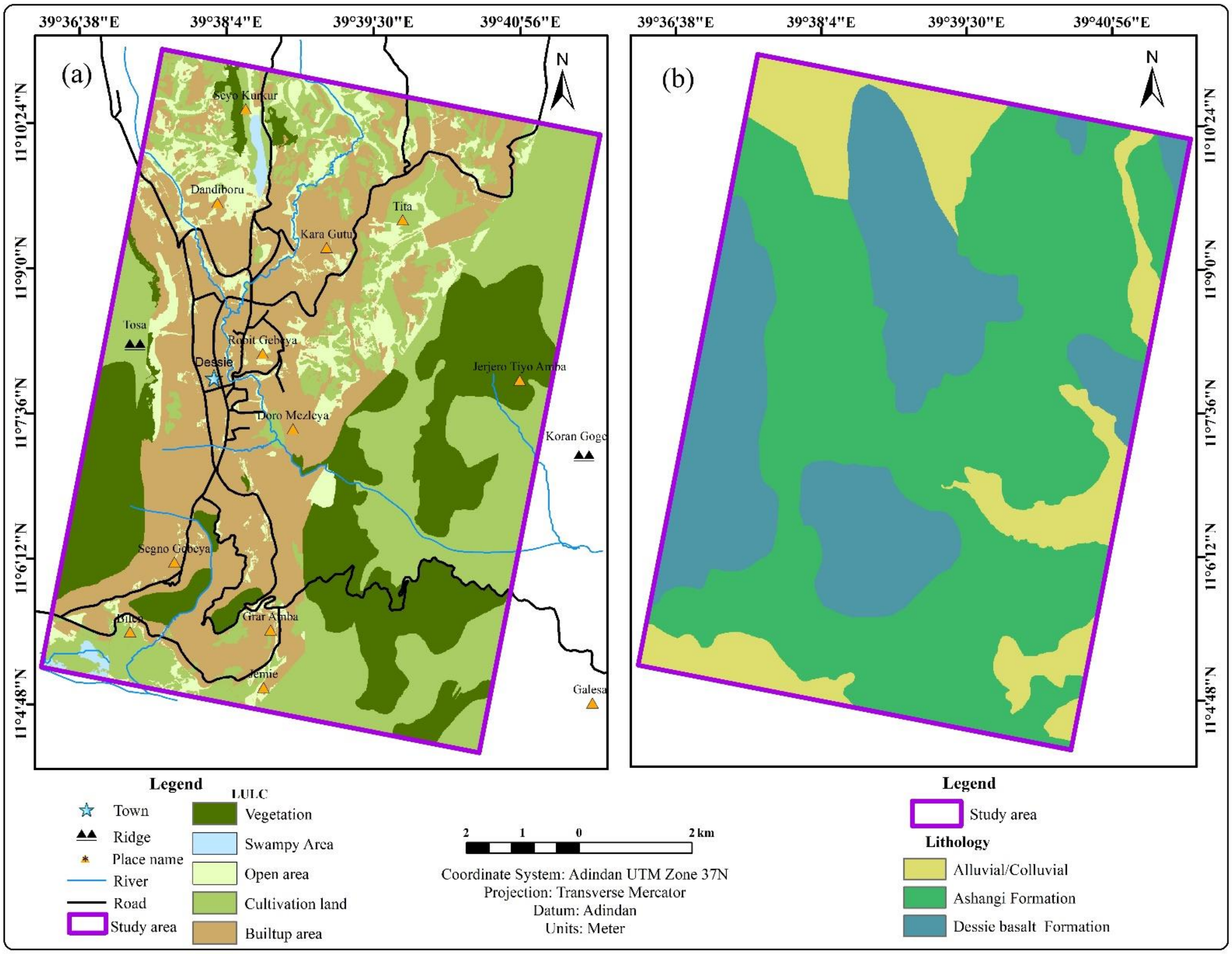

Figure 4.18 Land-use and land-cover map (a), and Lithology map (b)

4.3.7. Distance to road

In this study area, the distance from the road map was classified in to five ranges according to the euclidean distance analysis of the roads at an interval of 100-meter Fig. 4. 19a.in accordance to the study, proximity to the road causes the frequency rate of landslides to gradually reduce as the distance from the road increases. In this study, many landslides occur along the road due to improper rock cutting.

4.3.8. Distance to river

In the recent study, the distance from the river map was classified in to five ranges according to the euclidean distance analysis of the roads at an interval of 50-meter Fig. 4. 19b.proximity to rivers can increase landslide risk by weakening the soil's structure and causing mass movements during periods of high rainfall or flooding. In this study, many landslides occur along the river. Due to erosion, saturated soil, and water induced slope instability.

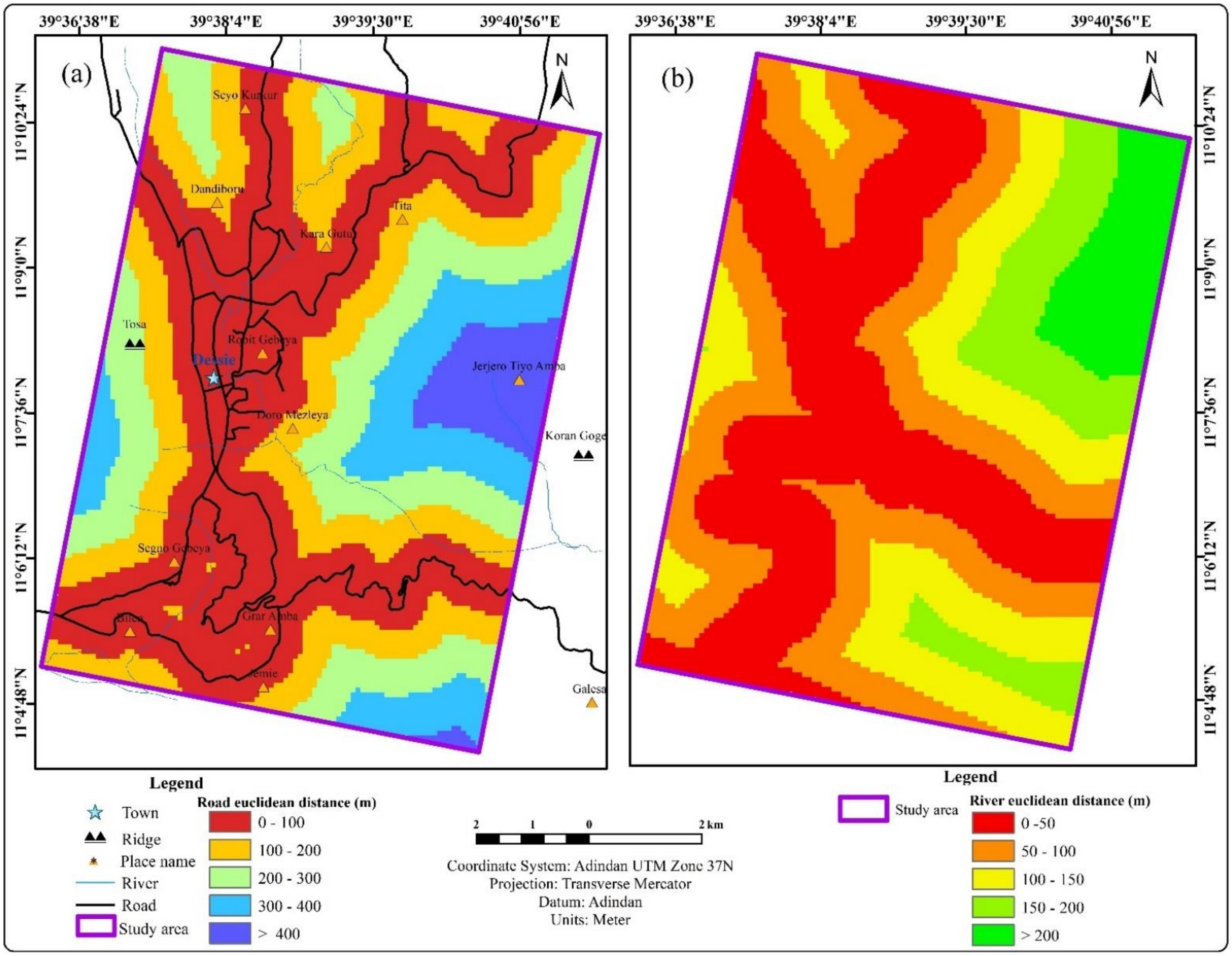

Figure 4.19. Road euclidean distance (a), and river euclidean distance (b)

4.4. Landslide hazard zonation map

The results for landslide zones were classified in to five distinct classes which is very low, low, medium, high and very high with 19.68%, 20.38%, 20.57%, 19.64%, and 19.71% respectively. The very high and high landslide hazard zonation classes found in the western, south western, central and eastern and north eastern part of the study area, the area coverage of landslide hazard zonation map classes very low, low, medium, high and very high with 1718.97 ha, 1780.18 ha, 1797.09 ha, 1716.19 ha and 1721.53 ha respectively. Fig. 4.20 give details of landslide hazard zonation final overlay of thematic layers result map and area coverage with percentage Present in Table 4.3.

Table 4.3. Landslide hazard zonation with percentage

LHZ classes	Area (ha)	Area (%)	Suitability rank
Very low	1718.97	19.68	1
Low	1780.18	20.38	2
Medium	1797.09	20.57	3
High	1716.19	19.64	4
Very high	1721.53	19.71	5

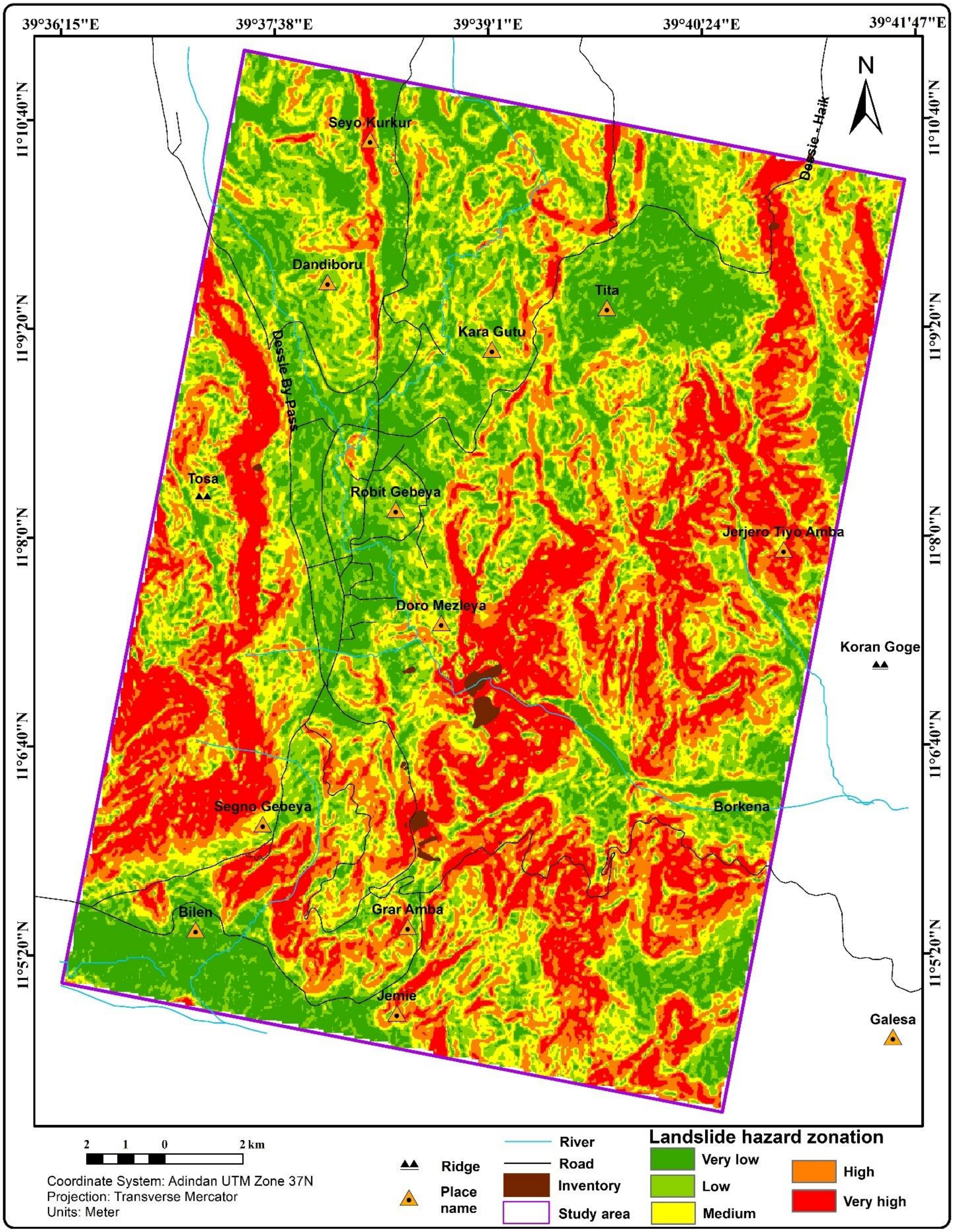

Figure 4.20 Landslide hazard zonation map

4.5. Validation or verification of landslide hazard zonation map

To ensure the accuracy of the LHZ detected by geographic information system (GIS) and remote sensing (RS) approaches, existing inventory data is taken into account. The final LHZ map includes field data from 15 existing inventory points. The landslide inventory points are located in very high, high and medium and low landslide hazard zonation map, with none in very low zones. This demonstrates that the approach used and the prevailing ground truth is in strong agreement. As indicated in Table 4.4 and 4.5. Landslide inventory points overlayed with LHZ map 66.67% of the inventory points is located in very high landslide hazard zone and 13.33% in high landslide hazard zone, 6.67% medium and low 13.33% respectively. And also inventory points overlayed with LHZ map present in Fig. 4.22. The results show that the LHZ detected by the GIS and RS approaches are accurate. The landslide hazard zonation was also evaluated using receiver operating characteristics (ROC) analysis, specifically by calculating the area under the curve (AUC), a common technique for measuring model accuracy. In ROC analysis, the AUC value indicates the model's accuracy, with an AUC of 1 representing perfect accuracy (Prasad et al., 2020). The ROC curve graphically represents specificity (false positive) on the X-axis and sensitivity (true positive) on the Y-axis. An AUC value greater than 0.7 is considered to demonstrate acceptable discrimination and satisfactory model performance (Iqbal et al., 2024). The landslide inventory data indicates very good model performance, failing with a range of 0.8−0.9 (0.81) or 81%, which is present in Figure 4.21. Therefore, the model demonstrates accuracy in delineating the landslide hazard zonation of the study area.

Table 4.4. Accuracy of inventory points overplayed with LHZ map

LHZ classes	Rank	LSHZ	Percent (%)
Very low	1	0	0
low	2	2	13.33
Medium	3	1	6.67
High	4	2	13.33
Very high	5	10	66.67

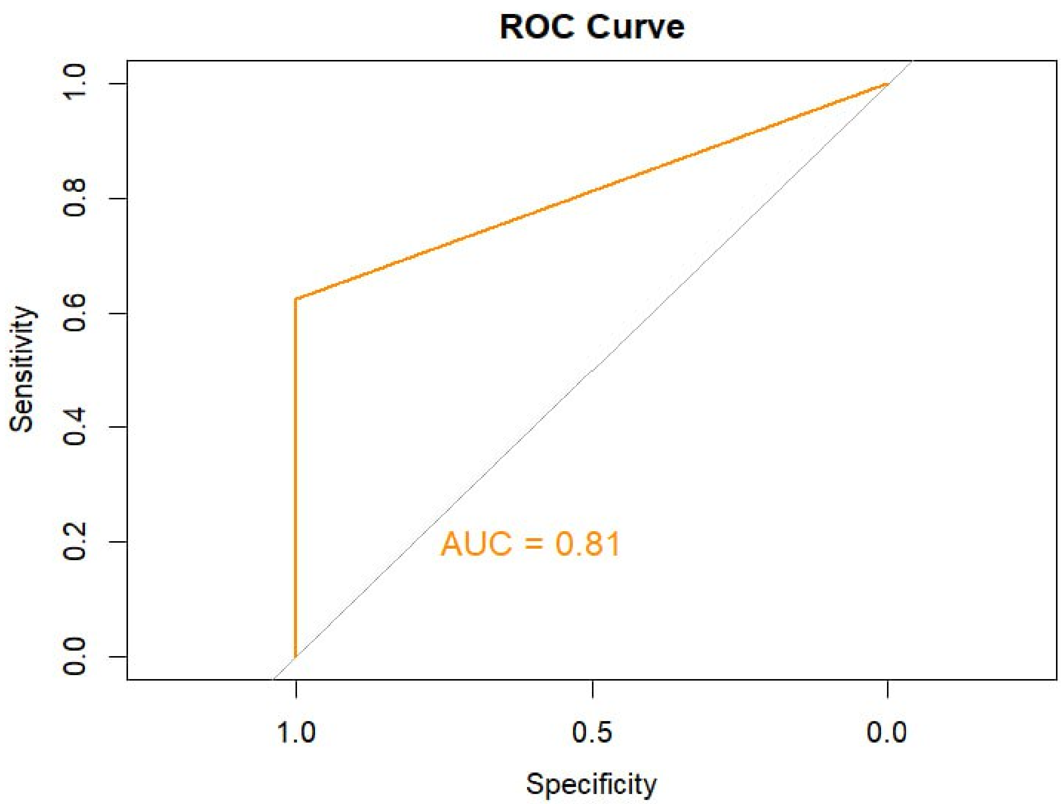

Figure 4.21. Validation of Landslide hazard zonation map

Table 4.5. LHZ map precision assessment with inventory

S/N	Inventory site	Location on LHZ map	Validation remark
1	Artificial landfill	Very high	Agree
2	Azwa gedel 1	Very high	Agree
3	Azwa gedel 2	Very high	Agree
4	Jamie sliding 1	Very high	Agree
5	Jamie sliding 2	Medium	Disagree
6	Road slide construction	Very high	Agree
7	Rock fall at menbere tsehay	Very high	Agree
8	Menbere tsehay spring and point	High	Agree
9	Doro mezileya	Low	Disagree
10	Menbere tsehay point 1	High	Agree
11	Harego	Very high	Agree
12	Tosa	Very high	Agree
13	Tita point 1	Very high	Agree
14	Tita point 2	Low	Disagree
15	Dessie adari school	Very high	Agree

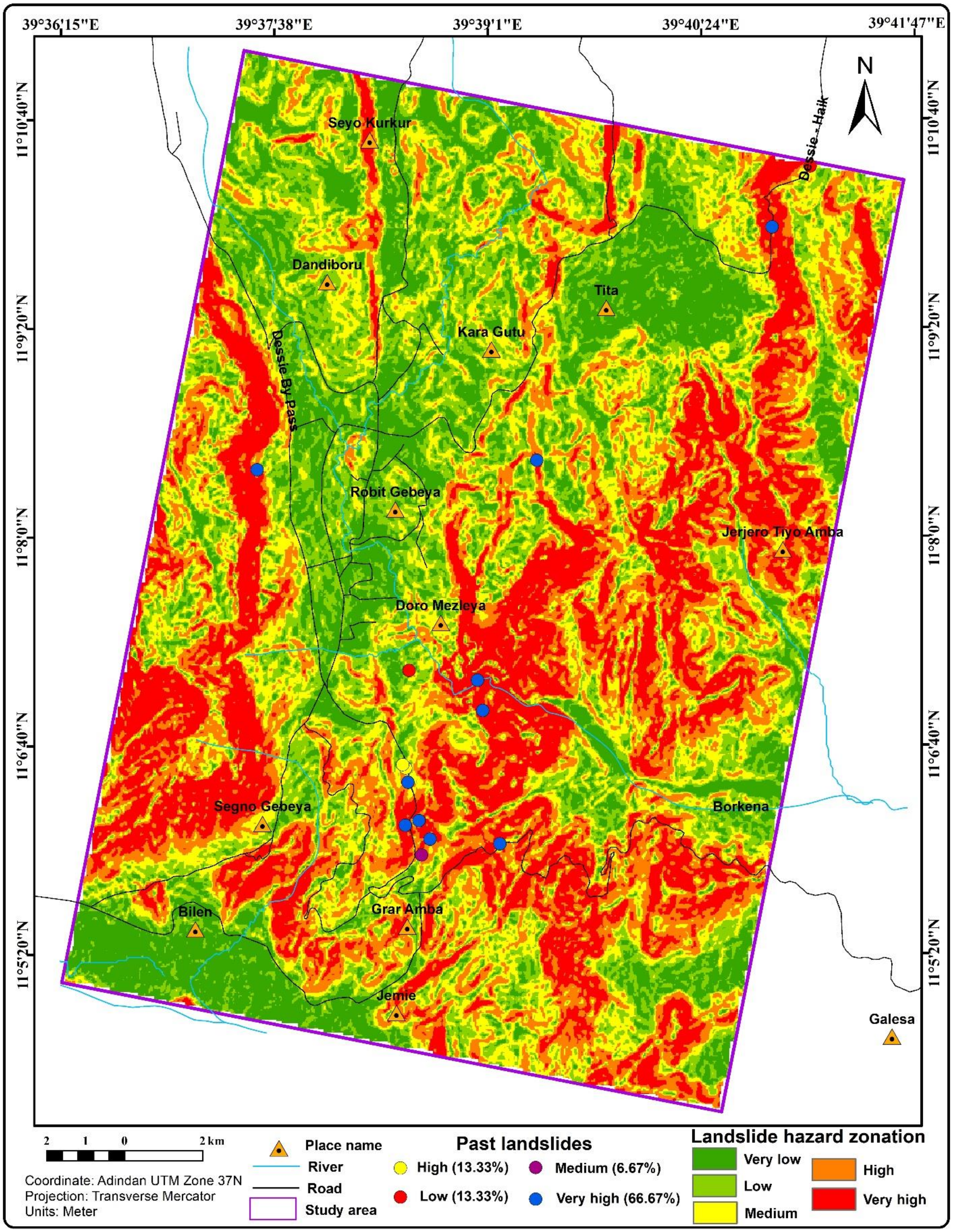

Figure 4.22. Validation of Landslide hazard zonation map

4.5 Discussion

One of the most hazardous and frequently occurring natural disasters is a landslide, which is typically triggered by various factors that vary depending on the location (Endashaw, 2020: Emmanouil et al., 2020). In the recent past landslides are a common environmental problem due to the progressive infrastructure development and urbanization in Ethiopia (Abebe et al.,2010: Endashaw, 2020). In study area, landslide have been common, causing destruction and damage to infrastructure, land, and buildings. Hence, to reduce the extent of the damage landslide, it is necessary to identify the common conditioning factors and delineate the area into different susceptibility classes This research aims prepare a landslide hazard zonation map using weighted overlay method and determine the deformation at mm level using the most harmonious and advanced InSAR process method which is PSInSAR. The slope, elevation, aspect, lithology, proximity to road, proximity to stream, rainfall, and LULC were considered to prepare the landslide hazard map of the study area. Weightage of each parameter were assigned based on their relative importance to the landslide occurrences. Subsequently, all the parameters were summed up and the final map were produced. Accordingly, five susceptibility zones were identified on the landslide hazard zone map which are very low, low, medium, high, and very high. The classification was made based on standard deviation. This system of categorizing has been reinforced because it is employed in studies and publications by (Agegnehu et al., 2023; Basharat et al., 2016; Mengistu et.al., 2019). Based on the processing result, it shows that: 1718.97, 1780.18, 1797.09, 1716.19 and 1721.53 hectors covered by very low, low, medium, high, and very high susceptibility respectively, and most of the high and very high hazard zone located on north east, central and south west parts of the study area, these areas are directly connected to the topography, indicating they are a steep and have rivers.

To validate the results of landslide susceptibility zones, a landslide inventory map was produced using fieldwork GPS point, records, satellite imagery and historical data (Fig.5.1). out of the total (15) landslide inventory points, 1718.97, 1780.18, 1797.09, 1716.19 and 1721.53 hectors covered by very low, low, medium, high, and very high susceptibility respectively. Therefore, 38.87% (3437.72 ha) of the existing landslide falls under high and very high hazard zones. This indicate that the proposed method in this study is accurately predicted the hazard class., which mean large percentages (80%) of inventory points in these high hazard zone, most of this inventory point in the study situated near to main road and river. According the processed statical analysis confirmed its effectiveness as a primary technique for estimating landslide hazard zone, similar work done by (Endashaw, 2020; Ahmed, 2020) has employed this approach on their studies and validate the findings.

In the present study PSInSAR, using Sentinel A1 SLC data, PSInSAR revealed active deformation zone throughout the study area. The PSInSAR analysis result show the existence of deformation by displacement which ranges from –19.5 to –64.1 millimeter per year (Fig.5.2). According to the analysis, in the study area, there is currently instability and a chance of landslides in the future. A similar study conducted in Birbir-mariam area and Arbaminch-Gidole Road, Southern Ethiopia, assessed slope instability using the PSInSAR technique. The first work was done by (Endashaw, 2020) in the Birbir-mariam area of the southern regional state, applying the PSInSAR technique with fifteen sentinel images and analyzing slop instability. The analysis result shows there is a displacement ranges from 15 to – 19 mm/year. While the second study done by (Mengistu et.al., 2019), apply the same technique using seven sentinel image deformation analysis, reveals displacement rates between +5 mm/year and –5.4 mm/year, suggesting slope instability and the possibility of future landslides in the area. The findings of these two studies in line with our results, the only deference with these studies. the present study process and analyze on licensed SARPROZ software, while these two studies processed and analyze their data by open access SNAP software.

Other scientific papers (Carolina, 2020; Ćwiąkała et.al., 2020; Stupar et al., 2020) indicates InSAR is the most commonly used method for measuring displacements caused by induced seismicity and other land movements. In general, PSInSAR analysis indicated areas experiencing active deformation, whereas landslide hazard zonation analysis identified landslide prone zones.

CHAPTER FIVE

5. Conclusion and recommendations

5.1 Conclusion

The study conducted in Dessie, Ethiopia, focuses on utilizing the PSInSAR method and Sentinel a SAR data to detect and map landslides in the study area. The primary objective of landslide hazard zonation map was to delineate the spatial distribution of landslide prone area and the PSInSAR method is to monitor which areas are actively deforming area.by employing remote sensing and GIS software such as SARPROZ, ArcMap, and Google Earth, along with SAR imagery data, DEMs, and field data, the study revealed significant findings. This comprehensive approach offers a robust framework for effective landslide hazard assessment in Dessie, Ethiopia, contributing to improved hazard management in the area.

The following are the conclusions that arise from the results and discussion:

- InSAR techniques combined with remote sensing and GIS software were effective in detecting and mapping landslides in Dessie, Ethiopia.
- Deformation in displacement rates ranges from –64.1mm to -19.8 mm/year subsidence, with a maximum velocity of 0.83 mm per year.
- The hazard zonation map shows 20.57% (1797.09 ha) covered by medium susceptibility, 19.64% (1716.19 ha) by high susceptibility, and 19.71 % (1721.53) by very high susceptibility.
- Deformation rates ranges from –64.1 mm to -19.8 mm/year, with areas of high and very high susceptibility identified.
- High hazard zones were predominantly located in specific topographical areas connected to the north-east, central, and south-west parts of Dessie.
- Validation results showed that 80 % of inventory points aligned with the high and very high hazard zones, which confirm the accuracy of the hazard zonation map.
- The comprehensive approach offers an inclusive framework for effective landslide hazard assessment and mitigation in Dessie, Ethiopia.

5.2. Recommendations

Based on the detailed study conducted in Dessie, Ethiopia, utilizing advanced InSAR techniques and remote sensing technology, the study finding provide valuable insights in to landslide dynamics in the area, it is crucial to have reliable and effective decision support technologies to help with the monitoring and management of landslides as well as land management, especially in considering of the limited financial resources available.

Those areas that fall in very high, high, and moderate hazard zones, where active deformation is observed, may probably face landslide occurrence and related slope instability problem in the future. Hence, it is recommended to properly utilize the output of this research work and reserve the landslide prone areas for vegetation. Some of the roads constructed along slopes need to be immediately repaired of need a retaining wall, especially on the main road from Dessie to Kombolcha and around the Borkena river, which need retaining walls, surface drainage, vegetation, and slope dressing.

Additionally, incorporating community-based early warning systems and capacity-building initiatives can help in reducing the vulnerability of the local population to landslides. Overall, this comprehensive approach combining scientific data with local knowledge can contribute to sustainable land management practices and disaster risk reduction strategies in Dessie, Ethiopia.

References

Abay, Asmelash. (2012). Landslide Susceptibility and Causative Factors Evaluation of the Landslide Area of Debresina, in the Southwestern Afar Escarpment, Ethiopia. Journal of Earth Science and Engineering. 2. 133–144.

Abbate, E., Bruni, P., & Sagri, M. (2015). Geology of Ethiopia: A Review and Geomorphological Perspectives. Landscapes and Landforms of Ethiopia, 33–64. https://doi.org/10.1007/978-94-017-8026-1_2

Addis, A. (2023). GIS-Based Landslide Susceptibility Mapping Using Frequency Ratio and Shannon Entropy Models in Dejen District, Northwestern Ethiopia. Journal of Engineering, 2023, 1–14. https://doi.org/10.1155/2023/1062388

Ahmed Abdikerim (2020), Landslide Hazard Zonation and Evaluation in and around Funyan Biro town (Gursum District), Hararghe Oromia, Eastern Ethiopia: using statistical approach AAU thesis work.

Amitrano, D., Di Martino, G., Guida, R., Iervolino, P., Iodice, A., Papa, M. N., Riccio, D., & Ruello, G. (2021). Earth Environmental Monitoring Using Multi-Temporal Synthetic Aperture Radar: A Critical Review of Selected Applications. Remote Sensing, 13(4), 604. https://doi.org/10.3390/rs13040604

Andnet Nigussie, Daniele Perissin and Tulu Besha, (2021) Determination of Crustal Deformation around Afar (Erta Ale) using Sentinel 1SAR Interferometry,

Andsera Adugna Mekonnen, Tarun Kumar Raghuvanshi, Karuturi Venkata Suryabhagavan, Tibebu Kassawmar,(2022), GIS-based landslide susceptibility zonation and risk assessment in complex landscape: A case of Beshilo watershed, northern Ethiopia, Environmental Challenges,V 8,2022,100586,ISSN 2667–0100, https://doi.org/10.1016/j.envc.2022.100586.

Arsenios Tsokas, Maciej Rysz, Panos M. Pardalos, Kathleen Dipple, (2022), SAR data applications in earth observation: An overview, Expert Systems with Applications, Volume 205, 117342, ISSN 0957-4174, https://doi.org/10.1016/j.eswa.2022.117342.

Asmelash Abay, Giulio Barbieri and Kifle Woldearegay (2019) GIS-based Landslide Susceptibility Evaluation Using Analytical Hierarchy Process (AHP) Approach: The Case of Tarmaber District, Ethiopia, Momona Ethiopian Journal of Science (MEJS), V11(1), 14-36, 2019 ©CNCS

Aswathi, J., Binoj Kumar, R. B., Oommen, T., Bouali, E. H., & Sajinkumar, K. (2022). InSAR as a tool for monitoring hydropower projects: A review.Energy Geoscience, 3(2), 160–171. http://doi.org/10.1016/j.engeos.2021.12.007

Awoke Feleke (2021), Landslide Hazard Zonation around Ameya Town Konta Special Woreda, South Nation Nationality People Region, Ethiopia AAU thesis work.

Ayalew, Lulseged & Yamagishi, Hiromitsu. (2005). The application of GIS-based logistic regression for landslide susceptibility mapping in the Kakuda-Yahiko Mountains, Central Japan. Geomorphology. 65. 15-31. 10.1016/j.geomorph.2004.06.010.

Ayenew, T. & Barbieri, G. (2005). Inventory of landslides and susceptibility mapping in the Dessie area, northern Ethiopia. 77, 1–15, https://doi.org/10.1016/j.enggeo.2004.07.002.

Azeze, Azemeraw. (2021). Landslide inventory, susceptibility, hazard and risk mapping. 10.13140/RG.2.2.22962.73924.

Basharat M, Shah HR, Hameed N. (2016) Landslide susceptibility mapping using GIS and weighted overlay method: A case study from NW Himalayas, Pakistan.

Bekele Abebe, Francesco Dramis, Giandomenico Fubelli, Mohammed Umer ,Asfawossen Asrat (2009),landslides in the Ethiopian highlands and the Rift margins. Afr. Earth Sci. doi: 10.1016/j.jafrearsci.2009.06.006 //////

Berardino, P., Fornaro, G., Lanari, R., & Sansosti, E. (2002). "A new Algorithm for Surface Deformation Monitoring Based on Small Baseline Differential SAR Interferograms." IEEE Transactions on Geoscience and Remote Sensing, 40(11), 2375-2383.

Beyene, G. (2016). Landslide Hazard Assessment and Zonation Using Bivariate Statistical Analysis Approach: - The Case Study in Gora Gommany Village and Surrounding Area in Aleltu District, North Showa Zone, Centeral Ethiopia.

Bouchra, A., Musta-pha, H., & Mohammed, R. (2020). D-InSAR Analysis of Sentinel-1 Data for Landslide Detection in Northern Morocco, Case Study: Chefchaouen. Journal of Geoscience and Environment Protection, 8, 84-103. https://doi.org/10.4236/gep.2020.87005

Carrión-Mero, P.; Montalván-Burbano, N.; Morante-Carballo, F.;Quesada-Román, A.; Apolo-Masache,B. (2021), Worldwide Research Trends in Landslide Science. Int. J. Environ. Res.Public Health, 18, 9445. https://doi.org/10.3390/ijerph18189445

Casagli, N., Intrieri, E., Tofani, V., Gigli, G., & Raspini, F. (2023). Landslide detection, monitoring and prediction with remote-sensing techniques. Nature Reviews Earth & Environment, 4(1), 51-64.

Cîmpianu, Cătălin I., Alin Mihu-Pintilie, Cristian C. Stoleriu, Andrei Urzică, and Elena Huţanu. (2021). "Managing Flood Hazard in a Complex Cross-Border Region Using Sentinel-1 SAR and Sentinel-2 Optical Data: A Case Study from Prut River Basin (NE Romania)" Remote Sensing 13, no. 23: 4934. https://doi.org/10.3390/rs13234934

Cong Dai, Weile Li, Dong Wang, Huiyan Lu, Qiang Xu, Ji Jian. (2021), Active Landslide Detection Based on Sentinel-1 Data and InSAR Technology in Zhouqu County, Gansu Province, Northwest China. Journal of Earth Science, 32(5): 1092-1103. doi: 10.1007/s12583-020-1380-0

Ćwiąkała P, Gruszczyński W, Stoch T, Puniach E, Mrocheń D, Matwij W, Matwij K, Nędzka M, Sopata P, Wójcik A. (2020) UAV Applications for Determination of Land Deformations Caused by Underground Mining.Remote Sensing. 12(11):1733. https://doi.org/10.3390/rs12111733

Dubey, S., Sattar, A., Goyal, M. K., Allen, S., Frey, H., Haritashya, U. K., & Huggel, C. (2023). Mass movement hazard and exposure in the Himalaya. Earth's Future, 11, e2022EF003253. https://doi.org/10.1029/2022.EF003253

Endashaw Debru (2020); Mapping landslide and modelling slope instability using optical and PS-insar TECHNIQUES, A case study in Birbir-Mariam Area of the Southern Regional State, Ethiopia, A Thesis in A Thesis in Geomatics and Geodesy, AAU 2020

ESA, (2018)b. Earth online. Missions. Sentinel-1 https://earth.esa.int

Fayera Gizawu (2020) Landslide Hazard Zonation Using Geospatial and Multi Criteria Decision Analysis Techniques in Gechi District, Western Ethiopia Jimma university

Ferretti, A., Prati, C., & Rocca, F. (2001). Permanent Scatterers in SAR Interferometry. IEEE Transactions on Geoscience and Remote Sensing, 39(1), 8-20.

Filagot, Mengistu & Suryabhagavan, Karuturi & Raghuvanshi, Tarun & Lewi, Elias. (2019). Landslide Hazard Zonation and Slope Instability Assessment using Optical and InSAR Data: A Case Study from Gidole Town and its Surrounding Areas, Southern Ethiopia. 3. 1-14. 10.21523/gcj1.19030101.

Francesco Ponziani, Pierpaolo Ciuffi, Benedikt Bayer, Nicola Berni, Silvia Franceschini, Alessandro Simoni, (2023), Regional-scale InSAR investigation and landslide early warning thresholds in Umbria, Italy, Engineering Geology, V327, 107352, ISSN00137952, https://doi.org/10.1016/j.enggeo.2023.107352.

Fubelli, G., Abebe, B., Dramis, F. & Vinci, S. (2008). Geomorphological evolution and present-day processes in the Dessie Graben (Wollo, Ethiopia).Catena, 75, 28–37.

Gebremicheal, S. (2017). Landslide Hazard Evaluation and Zonation In And Around Hagereselam Town, School Of Earth Sciences Landslide Hazard Evaluation And Zonation In And Around Hagereselam Town, Tigray, North Ethiopia School Of Earth Sciences.

Hanssen, R. F. (2001). "Radar Interferometry: Data Interpretation and Error Analysis." Springer Berlin Heidelberg. ISBN: 978-3-662-04636-9.

Henriques, Cristina & Zêzere, José & Marques, F. (2015). The role of the lithological setting on the landslide pattern and distribution. Engineering Geology. 189. 10.1016/j.enggeo.2015.01.025.

He, Peng, Zhaocheng Guo, Hong Chen, Pengqing Shi, Xiaolong Zhou, and Genhou Wang (2023). "Research and Application of Early Identification of Geological Hazards

Technology in Railway Disaster Prevention and Control: A Case Study of Southeastern Gansu, China" *Sustainability* 15, no. 24: 16705. https://doi.org/10.3390/su152416705

Höser, Thorsten. (2018). “Analysing Capabilities and Limitations of InSAR Using Sentinel-1 Data for Landslide Detection and Monitoring.” Master’s thesis, Bonn: Department of Geography, Bonn University.

Hrysiewicz, A., Wang, X. & Holohan, E.P. EZ-InSAR: (2023) An easy-to-use open-source toolbox for mapping ground surface deformation using satellite interferometric synthetic aperture radar. Earth Sci Inform 16, 1929–1945. https://doi.org/10.1007/s12145-023-00973-1

Hussin, Hamzah & Fauzi, Nurhazren & Jamaluddin, Tajul & Arifin, Mohd. (2017). Rock mass quality effected by lineament using rock mass rating (rmr)-case study from former quarry site. Earth Science Malaysia. 1. 13-16. 10.26480/esmy.02.2017.13.16.

Ignjatović Stupar, Danijela, Janez Rošer, and Milivoj Vulić. (2020). "Investigation of Unmanned Aerial Vehicles-Based Photogrammetry for Large Mine Subsidence Monitoring" *Minerals* 10, no. 2: 196. https://doi.org/10.3390/min10020196

Iqbal, M., & Ganaie, D. B. (2024). Groundwater potential assessment using analytical hierarchy-driven geospatial techniques: Baramulla, Kashmir valley, India. Sustainable Water Resources Management, 10(1), 19.

Jie Dong, Mingsheng Liao, Qiang Xu, Lu Zhang, Minggao Tang, Jianya Gong, (2018), Detection and displacement characterization of landslides using multi-temporal satellite SAR interferometry: A case study of Danba County in the Dadu River Basin, Engineering Geology,Volume,240,95-109,ISSN,0013-7952, https://doi.org/10.1016/j.enggeo.2018.04.015.

Korma, T. C. (2022). GIS-based landslide susceptibility zonation mapping using frequency ratio and logistics regression models in the Dessie area, South Wello, Ethiopia

Li YX, Zhang Y, Su XJ, Zhao FM, Liang YW, Meng XM, Jia J (2021) Early identification and characteristics of potential landslides in the Bailong River Basin using InSAR technique.

Natl Remote Sens Bull 25(2):677–690 (in Chinese). https://doi.org/10.11834/jrs.20210094

Lichuan Chen, Pengfei Liu, Weiming Liao, Kui Zhang, Fei He, Liang Zeng,(2020) Regional-scale detection of unrecorded landslides in mountainous terrains by using interferometric stacking technique IOP Conf. Ser.: Earth Environ. Sci. 570 042052 doi:10.1088/1755-1315/570/4/0420

Lissak, Candide & Bartsch, Annett & de Michele, Marcello & Gomez, Christopher & Olivier, Maquaire & Raucoules, Daniel & Roulland, Thomas. (2020). Remote Sensing for Assessing Landslides and Associated Hazards. Surveys in Geophysics. 41. 1-45. 10.1007/s10712-020-09609-1.

Liu, W., Zhang, Y., Meng, X. (2023). Forecast volume of potential landslides in alpine-canyon terrain using time-series InSAR technology: a case study in the Bailong River basin, China. Landslides. https://doi.org/10.1007/s10346-023-02135-2

Liu, Y.; Yang, H.; Wang, S.;Xu, L.; Peng, J. (2022)Monitoring and Stability Analysis of the Deformation in the Woda Landslide Area in Tibet, China by the DS-InSAR Method. Remote Sens. 14, 532. https://doi.org/10.3390/rs14030532

Lu, Zhong & Kwoun, Ohig & Rykhus, Russell. (2007). Interferometric Synthetic Aperture Radar (InSAR): Its Past, Present and Future. Photogrammetric Engineering and Remote Sensing. 73.

Lynn Highland and Peter Bobrowsky (2018). TXT-tool 0.001-2.1 Landslide Types: Descriptions, Illustrations and Photos. In: Sassa, K., et al. Landslide Dynamics: ISDR-ICL Landslide Interactive Teaching Tools. Springer, Cham. https://doi.org/10.1007/978-3-319-57774-6_1

Malaperdas, George & Panagiotidis, Vayia. (2018). The aspects of Aspect: Understanding land exposure and its part in geographic information systems analysis. Energy & Environment. 29. 0958305X1876632. 10.1177/0958305X18766322.

Marsala Vincenzo, Galli Alberto, Paglia Giorgio, Miccadei Enrico. (2019). Landslide Susceptibility Assessment of Mauritius Island (Indian Ocean) Geosciences; Basel 9(12), 493. doi:10.3390/geosciences9120493

Metych, Michele. "Natural disaster". *Encyclopedia Britannica*, 21 Dec. 2023, https://www.britannica.com/science/natural-disaster. Accessed .

Mo-Ewn XIE1, Fu-Xia LV1* Li-Wei Wang (2019), Laboratory Tests On E-Pellets Effectiveness For Ore Tracking, Mining Science, vol. 26, 91–108 doi: 10.5277/msc192607

Nanehkaran, Y.A.; Chen, B.; Cemiloglu, A.; Chen, J.; Anwar, S.; Azarafza, M.; Derakhshani, R. (2023), Riverside Landslide Susceptibility Overview: Leveraging Artificial Neural Networks and Machine Learning in Accordance with the United Nations (UN) Sustainable Development Goals. *Water*, *15*, 2707. https://doi.org/10.3390/w15152707

Nassir W. (2019) Structural Deformation Monitoring in Urban Area (Addis Ababa city) Using INSAR.

Natnael Agegnehu and Solomon Gerra (2023), Landslide Mapping Using InSAR and GIS Techniques: A Case Study at Debresina Area, Ethiopia Research Square.

Necula, N.; Niculit, ˘a, M.; Fiaschi, S.; Genevois, R.; Riccardi, P.;Floris, M. (2021)Assessing Urban Landslide Dynamics through Multi-Temporal InSAR Techniques and Slope Numerical Modeling. Remote Sens., 13, 3862. https://doi.org/10.3390/rs13193862.

Nseka D, Kakembio V, Mugagga F, et al. (2022) Implications of Soil Properties on Landslide Occurrence in Kigezi Highlands of South Western Uganda. Landslides. Intech Open. Available at: http://dx.doi.org/10.5772/intechopen.99865.

Offiong Victor Eyo, Surv P.E. Bassey, Tpl Dr. Emmanuel Agbor, Uzoezie, Arinze Destiny, (2018) The Legal and Planning Implication of Built-Up Area Encroachment on Vegetation Resource (Green Areas) – The Case of Calabar and Ikom Statutory Planning Areas, Journal of Law and Judicial System, V 1, Issue 3, , PP 9-20 ISSN 2637-5893 (Online)

Opoku, P. A., Shu, L., & Amoako-Nimako, G. K. (2024). Assessment of Groundwater Potential Zones by Integrating Hydrogeological Data, Geographic Information Systems, Remote Sensing, and Analytical Hierarchical Process Techniques in the Jinan Karst Spring Basin of China. Water, 16(4), 566.

Owczarz, K. (2020). A review of geodetic and remote sensing methods used for detecting surface displacements caused by mining. In IOP Conference Series: Earth and Environmental Science(Vol. 609, No. 1, p. 012076). IOP Publishing.

Pacheco Quevedo, Renata & Velástegui Montoya, Andrés & Montalvan-Burbano, Nestor & Morante, Fernando & Korup, Oliver & Rennó, Camilo. (2023). Land use and land cover as a conditioning factor in landslide susceptibility: a literature review.

Pardeshi, S.D., Autade, S.E. & Pardeshi, S.S. (2013) Landslide hazard assessment: recent trends and techniques. SpringerPlus 2, 523. https://doi.org/10.1186/2193-1801-2-523

Piccirillo, E.M. & Justin-Visentin, E. & Zanettin, B. & Joron, J.-L & Treuil, M. (1980). Geodynamic evolution from plateau to rift: Major and trace element geochemistry of the central eastern Ethiopian Plateau volcanics. N Jahrb Geol Paläont Abh. 158. 139-179.

Prasad, P., Loveson, V. J., Kotha, M., & Yadav, R. (2020). Application of machine learning techniques in groundwater potential mapping along the west coast of India. GIScience & Remote Sensing, 57(6), 735-752.

Psomiadis E, Charizopoulos N, Efthimiou N, Soulis KX, Charalampopoulos I. (2020) Earth Observation and GIS-Based Analysis for Landslide Susceptibility and Risk Assessment.ISPRS International Journal of Geo-Information.; 9(9):552. https://doi.org/10.3390/ijgi9090552.

Rida Bokhari, Hong Shu, Aqil Tariq, Nadhir Al-Ansari, Rufat Guluzade, Ting Chen, Ahsan Jamil, Muhammad Aslam (2023), Land subsidence analysis using synthetic aperture radar data, Heliyon, e14690, ISSN 2405-8440, https://doi.org/10.1016/j.heliyon.2023.e14690.

Ruzza, G.; Guerriero, L.; Revellino, P.; Guadagno, F.M. (2020) A Multi-Module Fixed Inclinometer for Continuous Monitoring of Landslides: Design, Development, and Laboratory Testing. *Sensors*, *20*, 3318. https://doi.org/10.3390/s20113318

Samuel Addisalem (2017), Slope Stability Analysis of Rainfall Induced Landslides A Case Study on Gohatsion - Dejen Road Abay Gorg thesis work Addis Ababa Science and Technology University.

Seda Çellek,(2019) Effect of Fault Distance on Landslide, ISAS 4 (1): 268-275, , Ankara, Turkey

Selamat SN, Majid NA, Taha MR, Osman A. (2022), Landslide Susceptibility Model Using Artificial Neural Network (ANN) Approach in Langat River Basin, Selangor, Malaysia. Land.; 11(6):833. https://doi.org/10.3390/land11060833.

Sim, K.B., Lee, M.L. & Wong, S.Y. (2022), A review of landslide acceptable risk and tolerable risk. Geoenviron Disasters 9, 3. https://doi.org/10.1186/s40677-022-00205-6

Solari, Lorenzo & Del Soldato, Matteo & Raspini, Federico & Barra, Anna & Bianchini, Silvia & Confuorto, Pierluigi & Casagli, Nicola & Crosetto, M. (2020). Review of Satellite Interferometry for Landslide Detection in Italy. Remote Sensing. 12. 1351. 10.3390/rs12081351.

Tarun Kumar Raghuvanshi, Lensa Negassa, P.M. Kala (2015),GIS based Grid overlay method versus modeling approach – A comparative study for landslide hazard zonation (LHZ) in Meta Robi District of West Showa Zone in Ethiopia, The Egyptian Journal of Remote Sensing and Space Science,V 18, Issue 2,2015,P235-250,ISSN 1110-9823,https://doi.org/10.1016/j.ejrs..08.001.

Tesfay Kiros Mebrahtu, Bedru Hussien, Andre Banning & Stefan Wohnlich. (2021), Predisposing and triggering factors of large-scale landslides in Debre Sina area, central Ethiopian highlands. Bull Eng Geol Environ 80, 365–383. https://doi.org/10.1007/s10064-020-01961-1.

Tilahun Hamza and Raghuvanshi, K. (2017). GIS based landslide hazard evaluation and zonation– A case from Jeldu District, Central Ethiopia. Journal of King Saud University – Science , 151–165.

Tilahun Mersha and Matebie Meten (2020), GIS-based landslide susceptibility mapping and assessment using bivariate statistical methods in Simada area, northwestern Ethiopia, Mersha and Meten Geoenvironmental Disasters

Tzouvaras, M., Danezis, C. and Hadjimitsis, D.G. (2020). Small scale landslide detection using Sentinel-1 Interferometric SAR coherence.Remote Sens., 12(10): 1560-1567”

United Nations Geological Survey Lynn Highland and Johnson, (2004); http://pubs.usgs.gov/fs/2004/3072/

United Nations Geological Survey, Types of landslides multimedia publications (2023) www.usgs.gov/media

Vařilová, Z., Kropáček, J., Zvelebil, J., Šťastný, M. & Vilímek, V. (2015). Reactivation of mass movements in Dessie graben, the example of an active landslide area in the Ethiopian Highlands. Landslides, 12, 985–996, https://doi.org/10.1007/s10346-015-0613-2

Varnes, D.J., 1978, Slope movement types and processes, in Schuster, R.L., and Krizek, R.J., eds., Landslides- Analysis and control: Transportation Research Board Special Report 176, National Research Council, Washington, D.C., p. 11-23

Wendim, Solomon & Woldearegay, Kifle & Mebrahtu, Gebreslassie. (2023). Causes, Failure Mechanisms and Susceptibility Zonation of Landslides along Gedo-Dilb Road Corridor, Northern Ethiopian. 10.21203/rs.3.rs-3030483/v1.

Yuxiao QIN, (2018) Demo: APS Estimation & Multi- temporal analysis with Sarproz. Sarproz processing tutorial series, Tutor. Exerc. 75.

Appendices

Appendix 1 landslides inventory field photo in the study area

Appendix 2 Table, dataset information of Sentinel1, 25 images

Acquisition Date	Polarization	Perpendicular base line (B)	Temporal base line (T)	Height ambiguity (H)
20170209_VV	VV	-61.463277	-1476.000289	0.125647
20170504_VV	VV	-69.352459	-1392.000267	0.029478
20180111_VV	VV	-1.739591	-1140.000204	0.025018
20180405_VV	VV	71.641716	-1056.000211	0.070554
20181225_VV	VV	-78.683790	-792.000120	0.021729
20190412_VV	VV	27.102879	-684.000135	0.055784
20191021_VV	VV	25.374911	-492.000030	0.055965
20191220_VV	VV	-3.177551	-432.000044	0.024980
20200301_VV	VV	17.488074	-360.000069	0.056885
20200524_VV	VV	-23.684399	-276.000035	-0.003239
20201003_VV	VV	-31.105387	-143.999956	0.000473
20201226_VV	VV	7.764693	-59.999976	0.007078

20210224_VV	VV	0.000000	0.000000	0.037103
20210320_VV	VV	75.243341	24.000000	0.021040
20210519_VV	VV	72.769287	84.000026	-0.003304
20211221_VV	VV	-42.949905	300.000091	0.065244
20220219_VV	VV	-90.067504	360.000066	0.017404
20220327_VV	VV	-44.468711	396.000070	-0.008326
20220514_VV	VV	-71.201806	444.000093	0.001123
20221122_VV	VV	-155.218606	636.000179	0.001918
20230109_VV	VV	1.773925	684.000146	0.047127
20230509_VV	VV	-67.841839	804.000154	-0.038391
20231129_VV	VV	48.451321	1008.000224	0.049006
20240104_VV	VV	4.703254	1044.000206	0.043718
20240409_VV	VV	-89.026187	1140.000202	0.068345

Table Pair-wise comparison matrix of thematic layers with AHP

Factors	Slope	Lithology	Rainfall	Elevation	LULC	Dist- river	Dist- road	Aspect
Slope	1	1	1	3	3	3	3	5
Lithology	1	1	1	3	3	2	3	3
Rainfall	1	1	1	3	3	3	3	3
Elevation	1/3	1/3	1/3	1	1	1	3	1
LULC	1/3	1/3	1/3	1	1	1	1	1
Dist- river	1/3	1/2	1/3	1	1	1	1	1
Dist- road	1/3	1/3	1/3	1	1	1	1	1
Aspect	1/5	1/3	1/3	1	1	1	1	1
sum	4.53	4.83	4.67	14	14	13	16	16

Table Relative weights of thematic layer classes

Factors	Category (class)	LHZ	Rank	weight	Weight %
Slope	0–8.82	Very low	1	0.2293	22.93
	8.83–17.3	Low	2		
	17.4–26.7	Medium	3		
	26.8–37.6	High	4		
	37.7–75	Very high	5		
Lithology	Dessie basalt formation	Very low	1	0.2033	20.33
	Ashangi Formation	Medium	3		
	Alluvial soil	High	4		
Rainfall	875–910	Low	2	0.2126	21.26
	911–945	Medium	3		
	946–980	High	4		
	981–1020	Very High	5		
Elevation	1930–2170	Very low	1	0.0709	7.09
	2180–2360	Low	2		
	2370–2530	Medium	3		
	2540–2730	High	4		
	2740–3030	Very high	5		
LULC	Vegetation	Very low	1	0.0708	7.08
	Open area	Low	2		
	Cultivation land	Medium	3		
	Built-up area	High	4		
	Swampy area	Very high	5		
Distance to river	0–50	Very high	5	0.0751	7.51
	50–100	High	4		

	100–150	Medium	3		
	150–200	Low	2		
	>200	Very low	1		
Distance to road	0–100	Very high	5	0.0709	7.09
	100–200	High	4		
	200–300	Medium	3		
	300-400	Low	2		
	>400	Very low	1		
Aspect				0.0671	6.71
	North	Very high	5		
	South	High	4		
	West	Medium	3		
	East	Low	2		
	Flat	Very low	1		

If the consistency ratio CR is < 0.1. The matrix is acceptable and overlay analysis can be done using ArcGIS Overlay analysis. In this study the CR is 0.004 which is less than 0.1. To calculate CR

CR= CI/RI

CI = lambda max 8.04-8/n-1

8.04-8/7

CI = 0.0057

n = 8

Lambda max = 8.04

CR = 0.004

RI= 1.41

Appendix 3 Figures

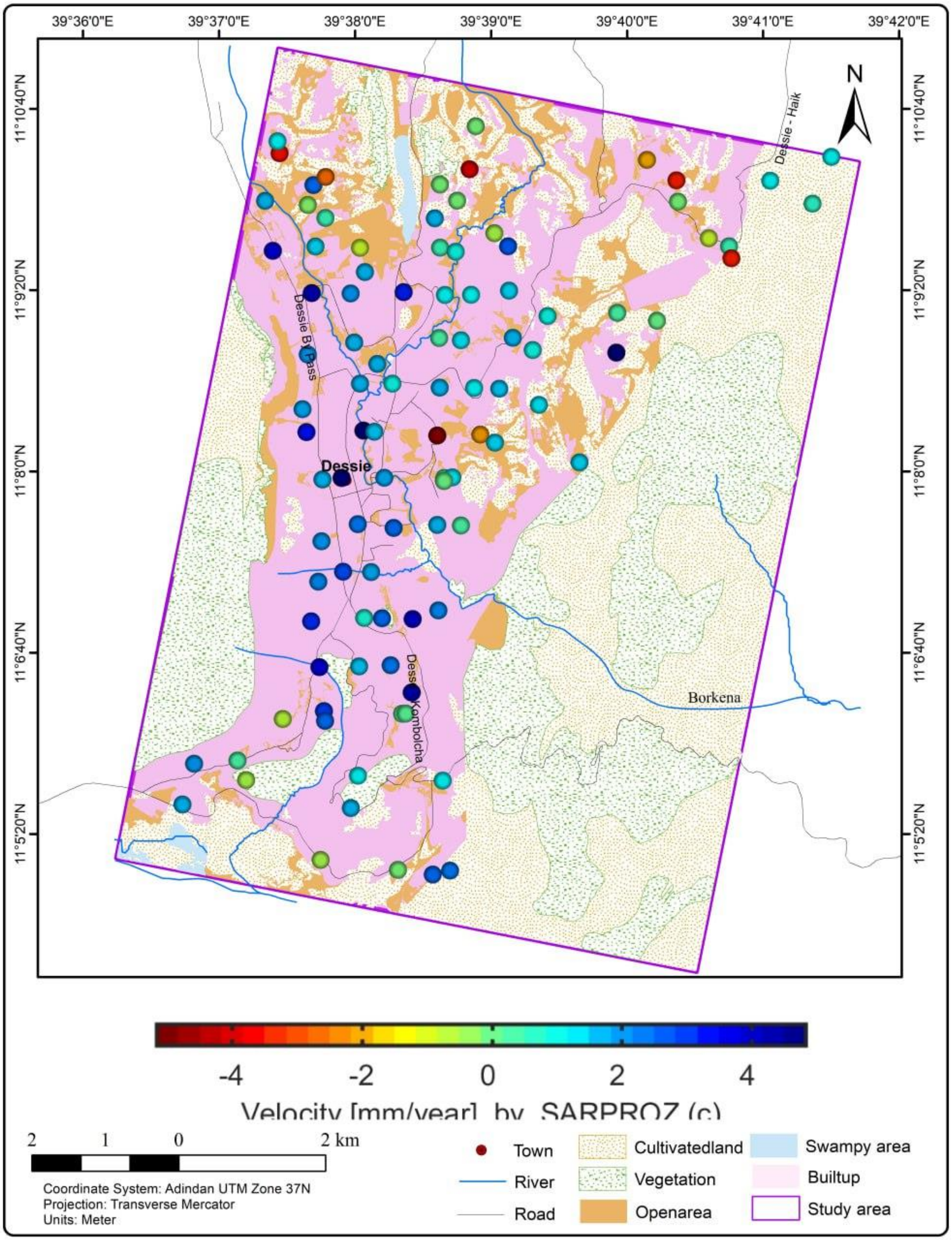

Figure 1 The deformation velocity of the study area obtained by PS-InSAR and Overlayed on study area LULC.

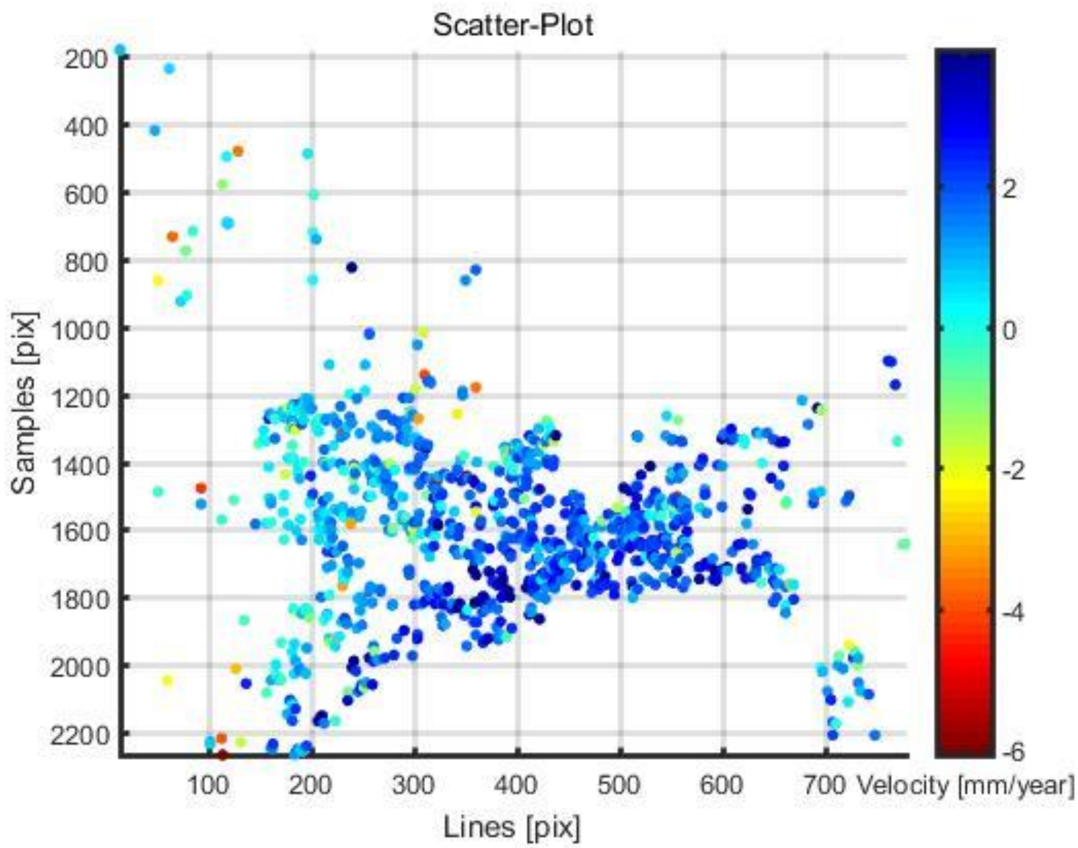

Figure 2 PS candidate of scatter plots